

Rockfall susceptibility and network-ranked susceptibility along the Italian railway

Massimiliano Alvioli*, Michele Santangelo, Federica Fiorucci, Mauro Cardinali, Ivan Marchesini, Paola Reichenbach, Mauro Rossi, Fausto Guzzetti, Silvia Peruccacci

Consiglio Nazionale delle Ricerche, Istituto di Ricerca per la Protezione Idrogeologica, via Madonna Alta 126, I-06128, Perugia, Italy

Abstract

Rockfalls pose a substantial threat to ground transportation, due to their rapidity, destructive potential and high probability of occurrence on steep topographies, often found along roads and railway routes. Various factors can trigger rockfalls, including intense rainfall and seismic activity, and diverse phenomena affect their probability of occurrence. Approaches for the assessment of rockfall susceptibility range from purely phenomenological methods and statistical methods, suitable for modeling large areas, to purely deterministic ones, usually easier to use in local analyses. A common requirement is the need to locate potential detachment points, often found uphill on cliffs, and the subsequent assessment of the runout areas of rockfalls stemming from such points.

Here, we apply a physically based model for the calculation of rockfall trajectories along the whole Italian railway network, within a corridor of total length of about 17,000 km and varying width. We propose a data-driven method for the location of rockfall source points based on expert mapping of potential source areas on sample representative locations. Using empirical distributions of gridded slope values in source areas mapped by experts, we derived probabilistic maps of rockfall sources in the proximity of the railway network, regardless of a particular trigger.

Source areas act as starting points of simulated trajectories, within the three-dimensional model STONE. The program provides a pixel-by-pixel trajectory count, which we classify into a susceptibility map. We obtained the map analyzing the railway track as a collection of segments, for which we provide segment-wise rockfall susceptibility.

Eventually, we considered an equivalent graph representation of the network, which helps classifying the segments both on the basis of rockfall susceptibility and the role of each segment in the network, resulting in a network-ranked susceptibility.

Keywords: Rockfall, Transportation Network, Physically Based Simulation, Rockfall Susceptibility

Contents

| | | |
|----------|---|----------|
| 1 | Introduction | 2 |
| 2 | Background | 2 |
| 2.1 | Physically based rockfall modeling | 2 |
| 2.2 | Analysis of the railway network within graph theory | 4 |
| 3 | Available Data | 4 |
| 4 | Methods | 6 |
| 4.1 | Identification of rockfall source areas | 8 |
| 4.2 | Simulation of rockfall trajectories with STONE | 11 |
| 4.3 | Analysis of the railway network within graph theory | 12 |
| 4.4 | Hardware and software settings | 13 |

| | | |
|----------|---|-----------|
| 5 | Results | 13 |
| 5.1 | Results of the procedure to identify source areas | 15 |
| 5.2 | Results for rockfall susceptibility within the model STONE | 16 |
| 5.3 | Impact of rockfalls on the railway network: network-ranked susceptibility | 18 |
| 6 | Discussion | 20 |
| 6.1 | Identification of rockfall source areas | 21 |
| 6.2 | The model STONE and rockfall susceptibility | 21 |
| 6.3 | Network-ranked rockfall susceptibility | 21 |
| 7 | Conclusions | 22 |
| 8 | Acknowledgments | 24 |
| 9 | Declaration of competing interests | 24 |

*Corresponding author

Email address:

massimiliano[dot]alvioli[at]irpi[dot]cnr[dot]it
(Massimiliano Alvioli)

Highlights

- We performed physically based rockfall susceptibility analysis along the Italian railway, over an area of size 25,400 km²
- Sample rockfall sources mapped by experts helped devising a probabilistic identification of potential sources in the whole area
- Locations of sources was a key input for three-dimensional simulation of rockfall runout areas within the STONE model
- We performed classification of railway segments into rockfall susceptibility classes and within a joint classification index including network properties

1. Introduction

Rockfall susceptibility along a transportation corridor is a recurring topic in landslide research. Conclusions based on quantitative studies are relevant for practical purposes, providing key information for risk mitigation. They may allow planning of protection barriers in key spots to optimize available resources and, as in the case motivating this work, they provide a quick estimate of the possible critical locations along a transportation network after a triggering event.

A susceptibility map does not contain information about the magnitude of possible events, nor their expected frequency over a period of time. Aiming to such a complete description (*i.e.*, a hazard map) would require knowledge of the processes responsible for the mobilization of individual blocks or rock masses at the local scale. That would demand a large body of data regarding the conditions of the rocks, at very high resolution and possibly in a multi-temporal way (Abellán et al., 2010; Giacomini et al., 2020), and deep understanding of the mechanism of sliding or detachment.

On the other hand, the input to prepare a susceptibility map is less demanding, though it would still not be trivial to gather the required data over a large area, as we aim to in this work. In order to estimate the likelihood of a particular location to be hit by a boulder falling from up-slope, the minimum requirement is knowledge of the point of origin of the falling mass, the underlying topography, and a model for the description of how the mass would reach a rest state, downhill.

A model to relate a rockfall source point with its end location should account for a three-dimensional trajectory resulting from the free fall, bouncing and rolling of individual boulders on a digital topography. Though phenomenological (easier) ways to accomplish the task exist, for example using an empirical shadow angle (*i.e.*, the angle between the distal limit of the shadow and the top of

the talus slope) (Evans and Hungr, 1993), here we committed to using the model STONE by Guzzetti et al. (2002). The model requires a digital elevation model (DEM) of the area, predetermined source locations, and numerical parameters controlling the energy restitution at the location of impacts of boulders with the topography. In principle, STONE allows the calculation of maximum velocity and maximum height of falling boulders, used in the literature to infer rockfall hazard (Guzzetti et al., 2003, 2004); we limited this study to susceptibility assessment. Thus, we only made use of the trajectory count per grid cell produced by the model.

To this end, in this paper we (i) applied a novel, data-driven method to specify source areas for rockfall trajectories (Alvioli et al., 2020b), based on expert-mapping of source areas in sample locations and statistical generalization across the whole study area; (ii) performed trajectory count simulation in a probabilistic way, using the model STONE, which we eventually classified as a susceptibility map along the national railway; (iii) performed a network analysis, within graph theory, trying to infer the impact of possible events on the functionality of the network as a whole. A national rockfall inventory consisting of more than 70,000 rockfall polygons helped in validating the results of this of this work in sample locations.

The paper is organized as follows. **Section 2** gives some context for this study, both for physically based rockfall modeling and for network analysis within graph theory. **Section 3** describes the data involved in this study. **Section 4** describes the core method, and it is split into three separate paragraphs describing how we singled out potential rockfall source locations, physically based rockfall susceptibility and analysis of the railway network within graph theory; an paragraph describes the computational demand of this work. Results and discussion are split in a similar way, in **Sections 5** and **6**, respectively. Conclusions are drawn in **Section 7**.

2. Background

2.1. Physically based rockfall modeling

Relevant stages of rockfalls are detachment of a rocky mass from a slope (usually a cliff face), typically by sliding, toppling or falling, and subsequent movement down slope, through a process which can assume different dynamics. These phenomena can vary among a rather broad spectrum, with two limiting cases represented by independent falls of individual fragments with no interactions among each other, and flow of granular masses with or without interaction with the substrate (Bourrier et al., 2013). Phenomena which do not fall strictly under the two limiting cases contain elements of both, and are the most difficult to model.

In this work we did not adopt a physical model for the detachment process. To our knowledge, no model exists that

would cover the multifaceted mechanism of initiation of a rockfall (Collins and Stock, 2016; Matasci et al., 2018). One possibility to avoid a detailed description of this step would be direct mapping through observation of the rocky slopes, for example by laser scanners (Jaboyedoff et al., 2012; Riquelme et al., 2014; Li et al., 2019), photogrammetry (Buyer et al., 2020), and similar approaches combined with remotely piloted aircrafts (Peréz-Rey et al., 2019; Santangelo et al., 2019; Giordan et al., 2020). Such measurements may provide detailed information about the fractured status and/or discontinuities of rocks, block orientations and distribution of joints, giving insight to infer locations of possible detachment areas (Turanboy et al., 2018). Recently, Mavrouli and Corominas (2020) devised a model to estimate the penetration of potential sliding planes within a rocky slope, based on a statistical method for evaluating the size of uninterrupted sequences of discontinuity planes on fractured slopes. The method allows to locate potential source areas, also estimating the potential for large volume failures. Eventually, Menegoni et al. (2021) introduced an algorithm to identify possible critical combinations between rock discontinuities and local orientation of the slope, to infer the possibility of failure even on large and complex areas.

The methods outlined above are only applicable on small areas, and probably to individual slopes. Expert-mapping of possible source areas by photo-interpretation (Santangelo et al., 2019, 2020) is another approach which can be very effective, and can be applied to relatively larger areas. In this work, we aim to a very large area assessment, so none of these methods could be applied. A promising method to this end could be a multivariate statistical regression technique as the one outlined by Rossi et al. (2021), which was not implemented here, since we selected a data-driven method (Alvioli et al., 2020b) described in the following sections.

Among the different cases outlined above for tracking the path of a rockfall, here we only deal with individual masses following independent trajectories. These can be described by ballistic dynamics, during free fall, and bouncing or rolling on the ground. In particular, the model STONE adopted here assumes point-like boulders under the only action of gravity and the constraints due to topography and geology. The computer program STONE models the motion of three possible states in a number of time steps in a three-dimensional fashion along the trajectory, until the motion comes to an end due to friction exhausting the initial kinetic energy.

Types of movements of rocky masses other than ballistic trajectories interrupted by bouncing or rolling are not included in this work, as they require models suited to describe avalanches and granular fluxes, while STONE does not include interactions between boulders, neither it accounts for their fragmentation. Recently, Matas et al. (2020) and Ruiz-Carulla et al. (2020) studied in detail the

fragmentation mechanism of large boulders by directly observing blocks debris after they impacted the slope. Data about the angular distribution of the fragments helped calibrating numerical parameters of the model RockGIS (Matas et al., 2017), which implements a fractal model for the mass of the fragments. They suggest the method be used after careful calibration of such parameters, in possible similar studies, due to the wide range of possible outcomes of the fragmentation mechanism.

To go beyond a spatial susceptibility assessment, one should consider the magnitude of possible rockfalls, in a given area, and their temporal recurrence. Magnitude may vary in a wide range of volumes, from cubic decimeters to millions of cubic meters (Hung et al., 1999). Corominas et al. (2018) recently showed that use of existing power law frequency-magnitude relations may be misleading in some cases, because magnitudes extrapolated outside of the range of observed data might actually never occur. This would be due to the non-existence in the study area of physical conditions – large rock masses, fracturing patterns – for such large volumes of rocks to develop into a rockfall. Melzner et al. (2020) also investigated frequency-size distributions, finding a dependence on the method used to map rockfalls and, similarly to Corominas et al. (2018), recommended caution when considering the large-size region of the distributions. We did not consider the magnitude of rockfalls, here, as the model STONE does not directly account for that.

We also did not account for a specific trigger: that could have limited the applicability and meaningfulness of the susceptibility map. As a matter of fact, rockfalls may be triggered by different phenomena, mostly by intense rainfall and seismic activity, with their occurrence influenced by a variety of factors. Static factors are steep terrain gradient and structural setting, and dynamic factors are thermal deformations and or freezing-thawing cycles of the rocks. Quantitative studies exist about correlations between rockfalls and rainfall, for example by means of probabilistic rainfall thresholds (Melillo et al., 2020). Previously, Delonca et al. (2014) studied the relation between rockfalls and rain, freezing periods, and strong temperature variations. They found a positive correlation between cumulative rainfall and rockfalls in one inventory, a correlation between cumulative rainfall and rockfalls in another inventory, and a correlation between the daily minimum temperature and rockfalls in a third one. Macciotta et al. (2015) performed a comprehensive analysis of rockfall triggers, including precipitation intensity, Snowbelt, seismic activity and occurrence of freeze-thaw cycles. They found evidence of correlation between rockfall occurrence and 3-day antecedent conditions of precipitation and freeze-thaw cycles.

Among examples of earthquake-induced rockfalls, Govi (1977) mapped landslides triggered by the earthquake of 1976 in Northern Italy, by means of systematic photo-

interpretation and field studies. The inventory contain mainly rockfalls, which frequently consisted of reactivation of phenomena which existed before the earthquake. Marzorati et al. (2002) considered the earthquake in Central Italy of 1997, and attempted to explain the distribution of rockfalls with statistical methods. Inclusion in our method of a trigger- or time-dependent description is also beyond the model STONE, thus it falls out of the scope of this paper and needs to be considered elsewhere.

2.2. Analysis of the railway network within graph theory

Graph theory is the mathematical representation of pairwise relations between a collection of objects, and a whole science of graphs exists with examples in a broad spectrum of theoretical and applied research (Chartrand et al., 1993). One of major field of application of graph theory is the representation of a physical network. Literature on network and/or graph science is extensive, and it deals with a variety of phenomena. Examples are biological and social networks, power grids, telecommunications and, obviously, the world wide web and transportation networks (Barthélemy, 2011). Studies related to transportation networks often involve urban settings, including interdependent and/or multi modal networks of different means of transportation. Common applications of network and/or graph theory are optimization problems, including shortest path search, maximum flow and minimum cost flow (Ahuja et al., 1993).

The effect of disruption of a number of vertices or edges was also investigated in the literature; Mattsson and Jenelius (2015) contains a review on the resilience of transportation networks. A few general results are that redundancy in a complex network is not sufficient for tolerance upon failure, while tolerance is much higher for networks exhibiting scale invariance (Albert et al., 2000). For example, this is the case for the world wide web (Cohen et al., 2000). On the other hand, scale-free networks are subject to disruption upon removal of a few of the relevant vertices. Also, the presence of loops makes a network resilient to damage and fluctuations in flow load (Katifori et al., 2010). Recently, Bassolas et al. (2020) investigated vulnerable spots in urban transportation in conditions of massive traffic, within an agent-based method and a multi-layered description. Dynamics of interdependent networks is such that removal of a critical number of nodes leads to cascade failures (Buldyrev et al., 2010). Communication networks also influence the structure of cities, as exemplified by Alvioli (2020), who used the road network as a starting point to define boundaries of urban agglomerations in Italy.

In this work, we use basic notions of graph theory, useful to make sense of the relevance of a particular edge of the graph within the graph as a whole. We refer to “network” as the collection of physical links (track segments) and nodes (stations or intersections), and to “graph” as

the equivalent representation of edges and vertices. Actually, equivalence between the physical network and its graph representation may be incomplete, in general: the elements of the physical network are associated with specific geographical locations, while the associated graph is an abstraction that only retains the topology of the physical network and, optionally, a few other quantities.

We further refer to betweenness centrality of vertices (Freeman, 1978) and edges (Lu and Zhang, 2013), a measure of centrality of each such element in the graph. Betweenness centrality (in the following, betweenness) of a vertex is given by the number of shortest paths going through the vertex, out of the total set of shortest paths connecting any two pair of vertices in the graph (all-to-all routes). In a similar way, we can define betweenness of edges. Values of betweenness of vertices and edges depend on the weights of edges in the graph. As the graph considered here is associated to a physical network, we weight edges with the actual length of railway links. Centrality of a vertex or an edge in the network gives a measure of its relevance for functioning of the network as a whole.

Eventually, we devised a new (simple) centrality index intended to quantify the impact on the network when one edge is removed, which mimics an interruption due to an external event. The new index helps performing a combined classification of the railway segments, based simultaneously on centrality of the segments and their rockfall susceptibility. A similar approach, namely calculation of network risk assessment combining exposure to link failures and identification of link importance, was proposed by Cats et al. (2016) for a multi-modal public transport network in the Netherlands.

3. Available Data

This work involved both material which was already available to us and newly developed maps. Among the exiting material, this study required (i) a digital elevation model, needed for the whole processing chain; (ii) a nation-wide inventory of rockfalls; (iii) a small-scale lithological map; (iv) a vector map of the railway network. Newly developed maps were a nation-wide slope unit and sample rockfall source area maps. Here follows a short description of such pieces of information.

- Digital elevation model. The highest resolution DEM available for the whole of Italy is TINITALY (Tarquini et al., 2007). The grid is 10 m x 10 m, in the reference system with EPSG:32633. **Figure 1** shows a shaded relief map based on the 25 m-resolution EU-DEM; its use in this work is limited to this figure.
- Inventory of landslide phenomena in Italy, known as IFFI (Trigila et al., 2010; ISPRA, 2018). The IFFI inventory contains over 620,000 landslide polygons,

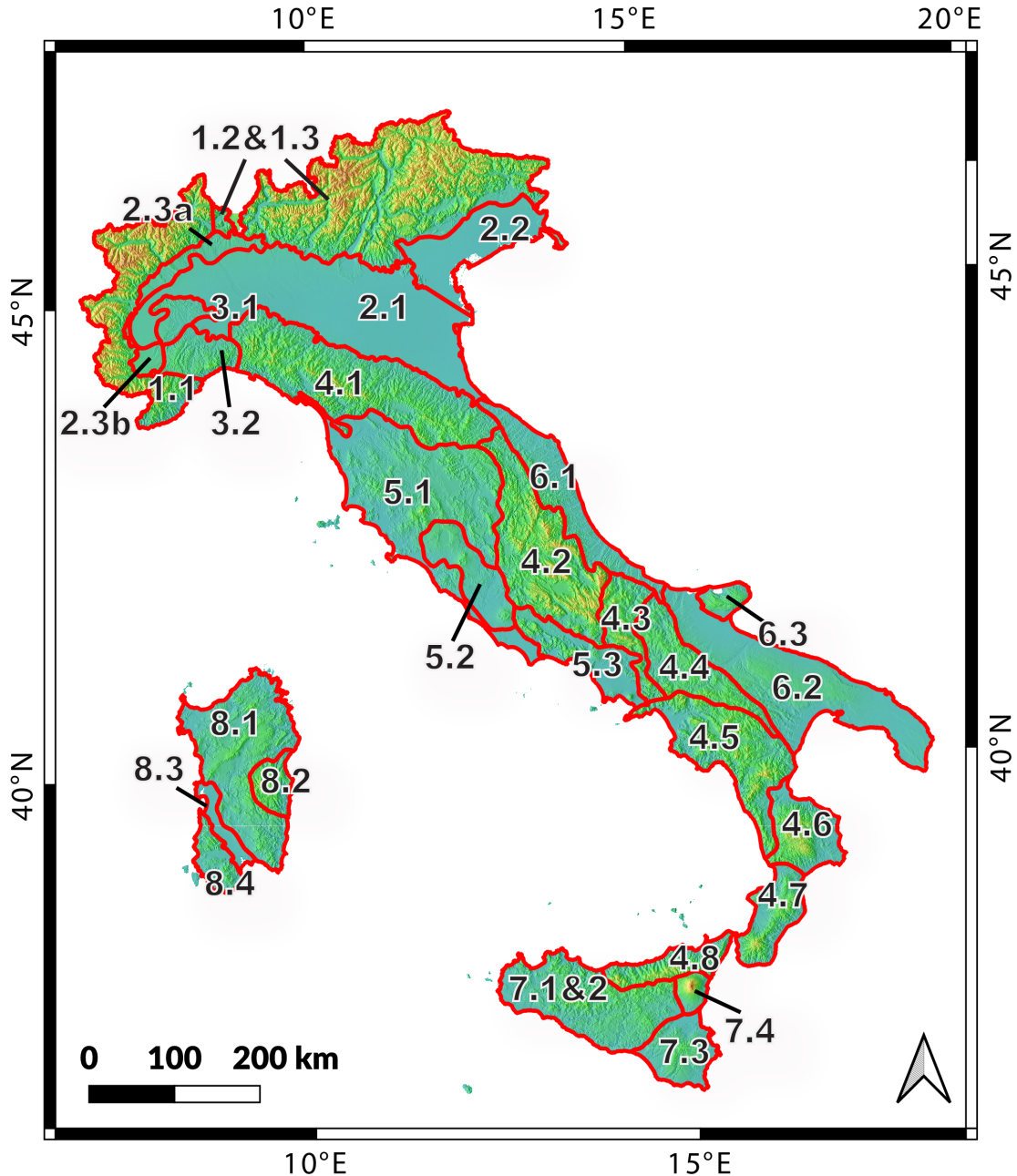


Figure 1: Map show boundaries of 29 topographic units in Italy, first defined by Guzzetti and Reichenbach (1994), with red lines, superimposed to a shaded relief calculated from the EU-DEM, 25 m resolution (after Alvioli et al. (2020a)). Code IDs of topographic units match the codes in **Tables 3** and **4**, while the units' names are listed in **Section 5.1**. Map is in EPSG:4326, datum in EPSG:3035.

of which 70,576 are classified as rockfalls, and 4,051 are located in the vicinities of the railway track and were used in this work. Rockfall polygons source and runout areas.

- Lithological map of Italy, scale 1:100,000 (Fongo, 2018; Bucci et al., 2021). **Figure 2** shows the map, with 19 lithological classes (**Table 1**).
- Map of subdivision in topographic units (TUs) of Italy (Guzzetti and Reichenbach, 1994).

- Nation-wide slope unit map (Alvioli et al., 2020a), also published in the research report “Unità territoriali di riferimento” P-05-1 of “Progetto RFI-SERVICE”, CNR IRPI, August 21, 2018. The map contains more than 300,000 slope unit polygons, of variable shape and size.

- Vector layer containing the railway network track. **Table 2** shows the distribution in elevation of the various links of the network, and **Fig. 3** shows the slope units selected from this work along the railway

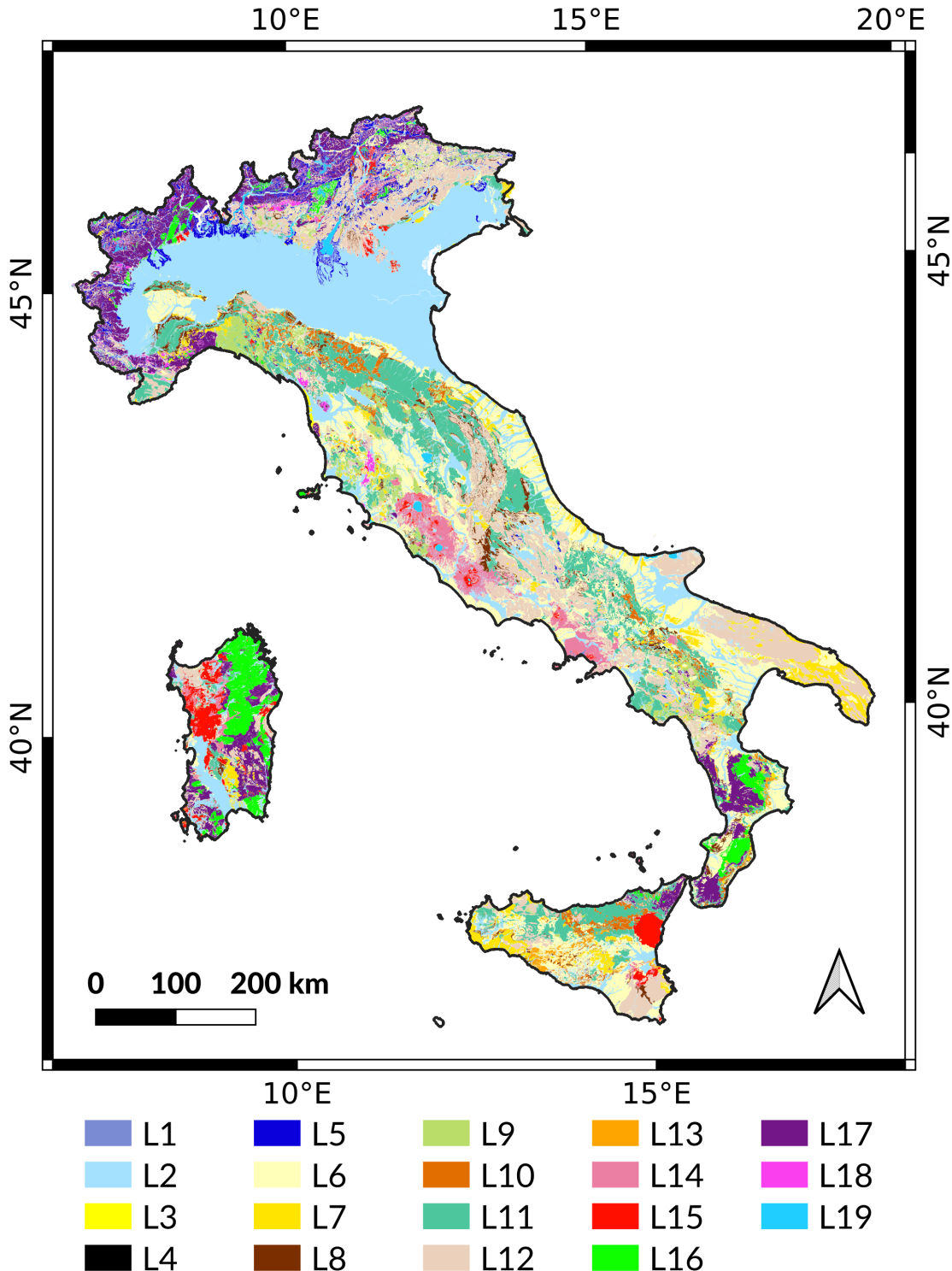


Figure 2: Lithological map. ID codes for the different lithologies match the codes in Table 1. After (Fongo, 2018; Bucci et al., 2021).

track. the figure also shows the track on plain areas, where slope units are undefined.

- A map of sample potential source area for rockfalls in Italy, from expert interpretation of Google Earth™ images.

4. Methods

Performing nation-wide rockfall susceptibility assessment, along the railway track, required careful planning. The long chains of actions, from data selection to the preparation of the final map, is in fact prone to propagating early-stage mistakes in unpredictable ways. Selection of

Table 1: Numerical values of the parameters used in STONE. Figure 2 shows the corresponding lithological map (Fongo, 2018; Bucci et al., 2021). STONE performs random sampling of values of the parameters in a $\pm 5\%$ range around the nominal values listed here.

| Class ID | Lithological Class | Dynamic Friction | Normal Restitution | Tangential Restitution |
|----------|--|------------------|--------------------|------------------------|
| L1 | Anthropic deposits | 0.65 | 35 | 55 |
| L2 | Alluvial, lacustrine, marine, eluvial and colluvial deposits | 0.80 | 15 | 40 |
| L3 | Coastal deposits, not related to fluvial processes | 0.65 | 35 | 55 |
| L4 | Landslides | 0.65 | 35 | 55 |
| L5 | Glacial deposits | 0.65 | 35 | 55 |
| L6 | Loosely packed clastic deposits | 0.35 | 45 | 55 |
| L7 | Consolidated clastic deposits | 0.40 | 55 | 65 |
| L8 | Marl | 0.40 | 55 | 65 |
| L9 | Carbonates-siliciclastic and marl sequence | 0.35 | 60 | 70 |
| L10 | Chaotic rocks, mélange | 0.35 | 45 | 55 |
| L11 | Flysch | 0.40 | 55 | 65 |
| L12 | Carbonate Rocks | 0.30 | 65 | 75 |
| L13 | Evaporites | 0.35 | 45 | 55 |
| L14 | Pyroclastic rocks and ignimbrites | 0.40 | 55 | 65 |
| L15 | Lava and basalts | 0.30 | 65 | 75 |
| L16 | Intrusive igneous rocks | 0.30 | 65 | 75 |
| L17 | Schists | 0.35 | 60 | 70 |
| L18 | Non-schists | 0.30 | 65 | 75 |
| L19 | Lakes, glaciers | 0.95 | 10 | 10 |

STONE as a rockfall runout modeling software (Guzzetti et al., 2002; Agliardi and Crosta, 2003) was dictated by the need to compromise between a well-defined relationship between sources and runout, and overall computational demand. Use of a physically based approach, capability of the program of running allowed to run simulations in a distributed way. We prepared data splitting the study area into sub-areas and work within sub-areas in parallel, computing-wise.

We adopted the topographic subdivision, previously defined by Guzzetti and Reichenbach (1994) and slightly modified for slope units delineation (Alvioli et al., 2020a). The original subdivision contained 30 sections, obtained by

quantitative analysis and visual interpretation of morphometric variables obtained from a digital elevation model. In the modified version, we neglected topographic units much smaller than the surrounding ones, and split one of the into two different ones, ending up with 29 topographic units, shown in **Fig. 1**.

A second, much finer subdivision of the territory was adopted here, consisting in groups of slope units intersecting the railway. The first subdivision (topographic units) was dictated by the need of similar terrain types, allowing to use the same soil parameters in each unit, for numerical simulations. The second was both a natural choice, given that slope units are mapping units well suited for landslide studies, and a solution to the technical problem of defining meaningful sub-areas for execution of the simulations in parallel.

Utilization of topographic domains also allowed us to define potential source areas of rockfalls using the statistical generalization proposed in this work separately within the 29 sections, corresponding to 29 different terrain types. A lithological map of Italy at the 1:100,000 scale provided the necessary insight for the determination of different sets of input parameters for the software STONE in different lithological classes. These parameters control the behaviour of boulders during rolling or bouncing on the ground, along the simulated trajectories. Their final values were inferred from previous studies.

To prepare a susceptibility map based on the results of the model STONE we adopted the following steps: (i) preparation of the data, (ii) selection of possible source areas,

Table 2: Distribution of the railway network in intervals of elevation. Total length is 17,727 km, a portion of which is outside of TINITALY DEM (denoted as N/A in the table), and the total number of segments is 3,419. Number of segments overlapping with at least one slope unit is 2,427, with total length 13,746 km.

| Elevation [m] | # Segments | Length [km] | Percentage |
|---------------|------------|-------------|------------|
| [0,100) | 1,746 | 8,671 | 45.0% |
| [100,500) | 1,447 | 7,814 | 46.5% |
| [500,1000) | 188 | 1,034 | 7.5% |
| [1000,2000) | 24 | 141 | 0.8% |
| [2000,3000] | 2 | 7 | 0.0% |
| N/A | 12 | 59 | 0.2% |

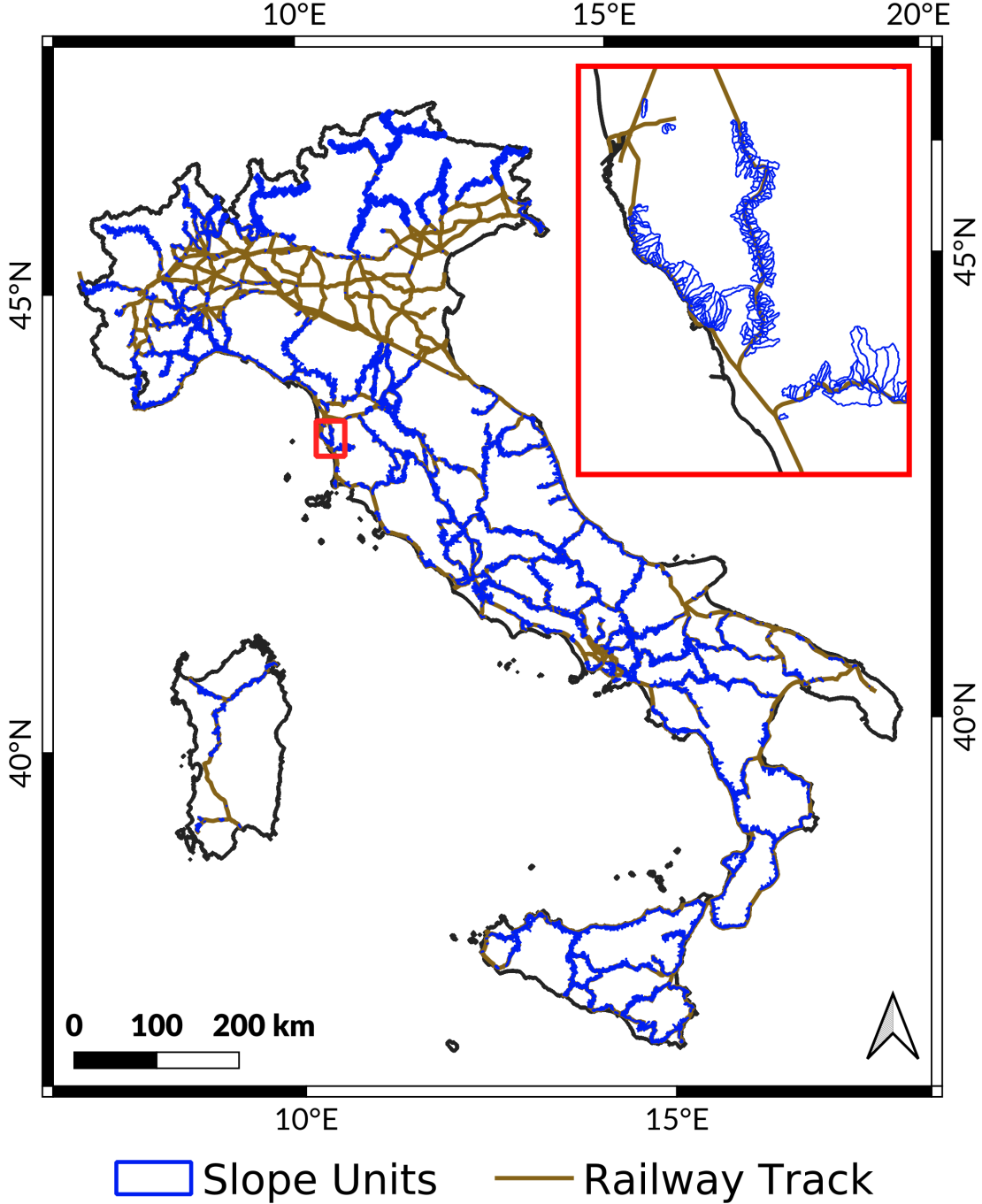


Figure 3: The spatial buffer along the railway network adopted in this work. The buffer consists of the subset of slope units from Alvioli et al. (2020a) intersecting a buffer of 1 km around the whole railway track, depicted in brown. Slope units are in blue. The total number of selected slope units is 32,200, out of the over 330,000 polygons, for a planimetric area of 25,400 km² (cf. Table 3).

which is probably the most important input of the model, (iii) execution of the program, (iv) collection and classification of the results analyzing the susceptibility results from the perspective of the properties of the network. The following paragraphs describe in detail all the steps performed in the analysis.

4.1. Identification of rockfall source areas

Identification of potential rockfall source areas is a key step of physically based simulation of rockfall runout, because they substantially influence the extent of runout. A detailed investigation of the location of potential sources of rockfalls requires expert analysis of the cliffs in the study area (Guzzetti et al., 2004; Santangelo et al., 2019, 2020), which is typically a time consuming and expensive procedure. This makes identification of potential sources a

limiting factor for systematic rockfall studies over large areas. Visual mapping of all of the potential sources by photointerpretation over the whole of the railway network in Italy would be impossible, in a reasonable time. Moreover, once a potential source is located on a DEM, it is desirable to assign a probability for the likelihood of that location to evolve into a rockfall.

A straightforward way of selecting source areas for STONE is to establish a slope threshold above which any grid cell acts as a potential rockfall source, (Guzzetti et al., 2003). Other criteria are based on a combination of geomorphological analysis and mapped sources (Agliardi and Crosta, 2003), a combination of a slope threshold and geomorphological analysis (Sarro et al., 2020), or a multivariate statistical analysis (Rossi et al., 2021). In this work, we adopted a method to both locate sources and assign a probability of failure in a homogeneous way over a large area, on the 10 m-resolution DEM of Italy (TINITALY, Tarquini et al. (2007)), according to the following steps:

- 1a. selection of a 1 km-wide buffer region around the railway track;
- 2a. selection of the subset of slope units (SU) intersecting the buffer, out of the whole set of about 330,000 SUs calculated for Italy by Alvioli et al. (2020a);
- 3a. expert mapping of potential rockfall source areas within the selected SUs, in sample locations we considered representative of the conditions that could trigger rockfalls in the specific topographic unit (Guzzetti and Reichenbach, 1994) under investigation;
- 4a. development of a data-driven procedure to identify source areas in different grid cells, with respect to the areas mapped as in 3a within the same topographic unit, using statistical generalization;
- 5a. visual analysis of the source areas map obtained from point 4a and assimilation in the final source area map of additional sources in locations chosen in expert way.

Selection of the SU overlapping with a 1-km buffer around the railway track (*cf.* point 1a) ensures that the simulations will include all of the potential sources that could develop into rockfalls and whose runout could concern the railway network (this work does not attempt to account for any anthropogenic mass displacements in the vicinities of the railway track). We favor SU as suitable mapping units for the description of landslide phenomena (Alvioli et al., 2016; Camilo et al., 2017; Schlögel et al., 2018; Bornaetxea et al., 2018; Tanyaş et al., 2019a,b; Jacobs et al., 2020; Amato et al., 2020; Chen et al., 2020; Li and Lan, 2020). More specifically, we adopted SUs instead of a geometric buffer around the track, because rockfall trajectories initiated in a given SU will be bounded within the SU, with reasonable confidence. The set of SU used here were specifically calculated and optimized over the whole of Italy (Alvioli

et al., 2020a) for this work, and for a series of additional works regarding selection of source areas of debris flows (Marchesini et al., 2020) and soil slides susceptibility (yet unpublished), along the railway network. The subset of SU selected for this work is shown in **Fig. 3**. The selected polygons (*cf.* point 2a) cover an overall area of 25,400 km².

We used the information of expert-mapped sources to calculate the probability of any grid cell to be a source as follows. For a given topographic unit, we selected SUs containing mapped polygons. We calculated histograms of the values of slope in the cells within the mapped polygons, and within the whole slope unit. For each bin of 2° width, we took the ratio of the two histograms: values of slope within the sources over values within the whole slope units. Since we took care of delineating all of the possible rockfall sources within each of the considered slope units, we are confident that the ratio represents the probability for a cell with slope in the 2° bin range of being a rockfall source, in that specific slope unit. This way, we have a probability point, for each 2° slope bin. Considering all of the sampled SUs in the given topographic unit, we end up with a collection of probability values as the green dots in **Fig. 4**, for TU 1.2 & 1.3, and of **Fig. 5** for all of the other TUs in **Fig. 1**.

The purpose of the procedure is to obtain probability-slope relations which can be extended to the entire set of selected SU, in each topographic unit. Green dots in **Figs. 4** and **Fig. 5** represent the probability values from expert mapping, and curves show three possible approaches to define a functional dependence between probability and slope. The black histogram is the simple average, in each slope bin, of the observed probability values. The blue curve is a non-linear fit of the values estimated from observed data, with a function of the following form:

$$P_{FIT}(S) = a \left(\frac{S}{90} \right)^b, \quad (1)$$

where S is the slope in degrees, and a, b are parameters of the fit. The band around the fit is the area between the minimum and maximum curves obtained using $a \pm \sigma_a$ and $b \pm \sigma_b$ (with $\sigma_{a,b}$ the standard deviations provided by least squares minimization), shown to illustrate goodness of fit. The red curve is a non-linear quantile regression with the 90th percentile, with a function containing a single parameter, c , as follows:

$$P_{QR}(S) = c \left(\frac{S}{90} \right)^4. \quad (2)$$

Thus, **Eq. (2)** is the curve dividing the observed sample in a way that 10% of the green dots in **Fig. 4** fall above the curve. We decided to use the method of quantile regression, **Eq. (2)**, to assign the probability of a grid cell to represent a source area (*cf.* point 4a). We believe that it maximizes the information extracted from observed data,

Table 3: Numerical evaluation of the statistical generalization for the probability of grid cells to initiate a rockfall trajectory. We list the total area of each section (Section ID, as in Guzzetti and Reichenbach (1994)), the area covered by slope units selected for this work Alvioli et al. (2020a), the number of expert-mapped source polygons and their total area. HR is hit rate (or true positive rate), the ratio $TP/P = TP/(TP+FN)$. “Mapped” refers to the cells underlying the expert-mapped source areas (colored in green-yellow-orange-deep orange, from high to small HR), and “IFFI” (colored in light to deep blue from large to small HR) refers to cells in the 90th elevation percentile of the rockfall polygons in the national inventory (Trigila et al., 2010).

| Section ID | Total Area [km ²] | SU Area [km ²] | Mapped Polygons (#) | Mapped Area [km ²] | HR (Mapped) (Total) | HR (Mapped) (P > 80%) | HR (IFFI) (Total) | HR (IFFI) (P > 80%) |
|--------------------|-------------------------------|----------------------------|---------------------|--------------------------------|---------------------|-----------------------|-------------------|---------------------|
| 1.1 | 16,274 | 1,590 | 152 | 3.2 | 77% | 13% | 86% | 23% |
| 1.2&1.3 | 35,735 | 2,620 | 78 | 2.2 | 80% | 19% | 76% | 10% |
| 2.1 | 32,702 | 373 | 11 | 0.039 | 80% | 27% | 63% | 8% |
| 2.2 | 9,426 | 164 | 38 | 0.58 | 11% | 6% | 72% | 11% |
| 2.3a | 3,103 | 458 | 58 | 0.34 | 75% | 16% | 87% | 12% |
| 2.3b | 1,298 | 88 | 2 | 0.001 | - | - | - | - |
| 3.1 | 2,322 | 332 | 39 | 0.027 | 16% | 0% | 100% | 100% |
| 3.2 | 3,991 | 1,778 | 225 | 0.84 | 51% | 4% | 29% | 1% |
| 4.1 | 22,393 | 2,067 | 151 | 0.84 | 78% | 7% | 60% | 15% |
| 4.2 | 16,835 | 1,894 | 105 | 1.5 | 79% | 9% | 59% | 5% |
| 4.3 | 4,920 | 457 | 89 | 1.9 | 77% | 13% | 77% | 13% |
| 4.4 | 8,097 | 1,585 | 102 | 1.6 | 75% | 14% | 46% | 6% |
| 4.5 | 12,890 | 1,379 | 200 | 7.2 | 79% | 18% | 62% | 11% |
| 4.6 | 6,203 | 383 | 62 | 0.34 | 50% | 3% | 44% | 1% |
| 4.7 | 5,337 | 598 | 70 | 0.57 | 59% | 9% | 46% | 3% |
| 4.8 | 4,262 | 511 | 127 | 1.6 | 48% | 3% | 30% | 7% |
| 5.1 | 25,346 | 2,086 | 80 | 0.19 | 58% | 12% | 44% | 6% |
| 5.2 | 6,136 | 972 | 11 | 0.013 | 79% | 5% | 16% | 1% |
| 5.3 | 6,375 | 859 | 81 | 0.081 | 62% | 4% | 59% | 6% |
| 6.1 | 9,023 | 930 | 46 | 0.035 | 78% | 10% | 42% | 100% |
| 6.2 | 20,236 | 706 | 107 | 1.2 | 44% | 11% | 38% | 11% |
| 6.3 | 1,731 | - | 0 | - | - | - | - | - |
| 7.1&7.2 | 14,285 | 2,195 | 121 | 3.5 | 56% | 12% | 33% | 6% |
| 7.3 | 5,321 | 691 | 561 | 0.97 | 46% | 9% | 34% | 5% |
| 7.4 | 1,499 | 210 | 31 | 0.37 | 80% | 28% | 100% | 100% |
| 8.1 | 16,404 | 428 | 80 | 1.4 | 63% | 14% | 25% | 2% |
| 8.2 | 258 | - | - | - | - | - | - | - |
| 8.3 | 1,946 | 4 | 6 | 0.061 | 58% | 21% | 41% | 18% |
| 8.4 | 2,844 | 42 | 11 | 0.66 | 76% | 22% | 63% | 13% |

with respect to the average and the fit of **Eq. 1**. Moreover, we used a function with a fixed exponent (the fourth power of $S/90$) because using a parametric exponent as in **Eq. (1)** the resulting curves systematically underestimated the probability of source presence for large values of slope. The procedure provides an individual curve $P_{QR}(S)$ for each topographic unit, obtained from expert mapping of potential rockfall source areas and from non-linear quantile regression of probability values observed in the same topographic unit.

In each topographic unit, cell-by-cell values of probability obtained from **Eq. (2)** were directly related with the number of simulated trajectories considering the cell as the starting point of a falling boulder. We imposed a lower threshold probability under which the cell is not considered as a source. The threshold is the minimum between the value of P_{QR} providing a source map covering at least 80% of the sources mapped by visual interpretation, and $P_{QR} = 10\%$. We simulated for each source cell a number of trajectories corresponding to the numerical value

of P_{QR} in percent; for example, a cell with probability X% would trigger X simulated trajectories. This allows to exploit the possibility in STONE of simulating a different number of falling boulders based on the probability of a given cell to be a source area. This method increases the degree of randomization of the simulations (together with the random selection of the value of input parameters within a given percent around the mean value provided as an input, built-in in STONE).

Figure 5 shows the P_{QR} relations for all of the topographic units used in this work as homogeneous domains simulation with STONE. Once source areas and the associated probabilities were estimated, we visually checked that no evident errors existed along the entire railway track (*cf.* point 5a). We systematically checked the results of the statistical classification of source areas along the entire railroad network, through expert visual analysis. In a few selected locations, in which expert geomorphologists considered that the infrastructure was potentially subject to manifest risk, additional source areas were delineated.

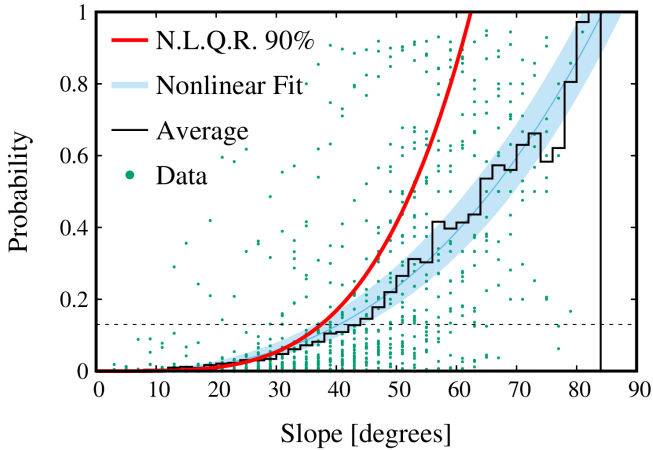


Figure 4: Example result of statistical assessment of the probability of a grid cell with given slope to represent a source area for rockfalls. Data (green dots) and numerical models (curves) correspond to topographic unit 1.2 & 1.3 in Figs. 1 and Table 1. The red curve, a non-linear 90% quantile regression corresponding to Eq. (2), is the adopted model. The horizontal line represents the limit under which probability is set to null.

In fact, the nature of the procedure did not guarantee absence of false negatives, required by the operational aim of the project.

4.2. Simulation of rockfall trajectories with STONE

After the selection of source areas, we performed the following steps to calculate rockfall susceptibility within a polygonal buffer around the whole Italian railway network, using the program STONE and the 10 m-resolution DEM used to identify sources of rockfalls:

- 1b. attribution of dynamic friction, normal and tangential restitution coefficients values, necessary for execution of the program STONE. This step was performed by expert assignment of values of coefficients available from the literature to each lithological class;
- 2b. preparation of data grids necessary for execution of STONE in each topographic unit, further split in rectangular domains containing contiguous SU polygons, as selected at point 2a in **Section 4.1**;
- 3b. execution of actual simulations with STONE. We performed distributed (parallel) runs within the 921 sub-areas described in point 2b;
- 4b. collection on the various raster maps containing the trajectory count per grid cell (“counter”), in each of the sub-areas of each of the 29 topographic units;
- 5b. transformation (classification) of the counter map into a probabilistic map.

Numerical values of dynamic friction, tangential and normal restitution are necessary for running the program STONE (*cf.* point 1b). We selected them as follows. We considered a lithological map at 1:100,000 scale, obtained

from a digital map in vector format. The original map, from Italian Geological Service (ISPRA (Tacchia, 2004; Battaglini et al., 2012)), contained more than 5,000 unique descriptions of geological formations (Fongo, 2018; Bucci et al., 2021). Using expert criteria, with the help of about 400 geological sheets (digital photographs from the same source) at higher scale, the original unique description were classified into 19 lithological categories. The numerical values of coefficients to run the program STONE were obtained using previous estimations for similar lithologies available in the literature. (Guzzetti et al., 2002, 2003, 2004; Agliardi and Crosta, 2003; Santangelo et al., 2019). The values selected are listed in **Table 1**.

The actions of points 2b, 3b, 4b were performed in 921 sub-areas singled out by considering separately groups of adjacent SUs: (i) a DEM of the sub-area under investigation; (ii) a grid containing the positions of the rockfall source areas, specifying the number of trajectories to be simulated; (iii) three grids, containing the values of dynamic friction and of normal and tangential restitution coefficients, for each grid cell of the DEM.

The software STONE produces as an output three grids containing: (a) a count of the number of trajectories that crossed the cell during the simulations; (b) the maximum height of the trajectories, measured from the local elevation; (c) the maximum velocity of the simulated boulders in each cell. The three grids can be used jointly, in principle, to estimate rockfall hazard in each cell. As a matter of fact, for given source areas, (a) can be interpreted as the relative probability of having a trajectory crossing each grid cell, while (b) and (c) may be jointly considered as a proxy of the magnitude of the expected rockfalls in each cell. Estimating temporal frequency of rockfall events, instead, requires additional information (Guzzetti et al., 2003, 2004). In this work, we only used output (a), as an estimate of the relative spatial probability of rockfall events.

To convert the trajectory count per cell into a probabilistic index (*cf.* point 5b) we used the following rationale. We considered the national inventory of landslide phenomena in Italy (IFFI - ISPRA (2018) and Trigila et al. (2010)). We extracted polygons labeled in the inventory as “falls” or as “extended areas containing falls”. We calculated empirical cumulative distribution functions (ECDFs) of the trajectory count, limited to the grid cells underlying the polygons extracted from IFFI inventory. In this way, we considered as relevant only the cells known to actually contain a rockfall. We used the ECDF to map all of the cells in the trajectory count grid with non-null value onto the [0,1] interval, which allows a probabilistic interpretation required for susceptibility map.

Using an ECDF, instead of a simple normalization of the trajectory count values, has two advantages. First, it allows to attribute less relevance to cells with a small number counts, given the huge variance of the counts in the output

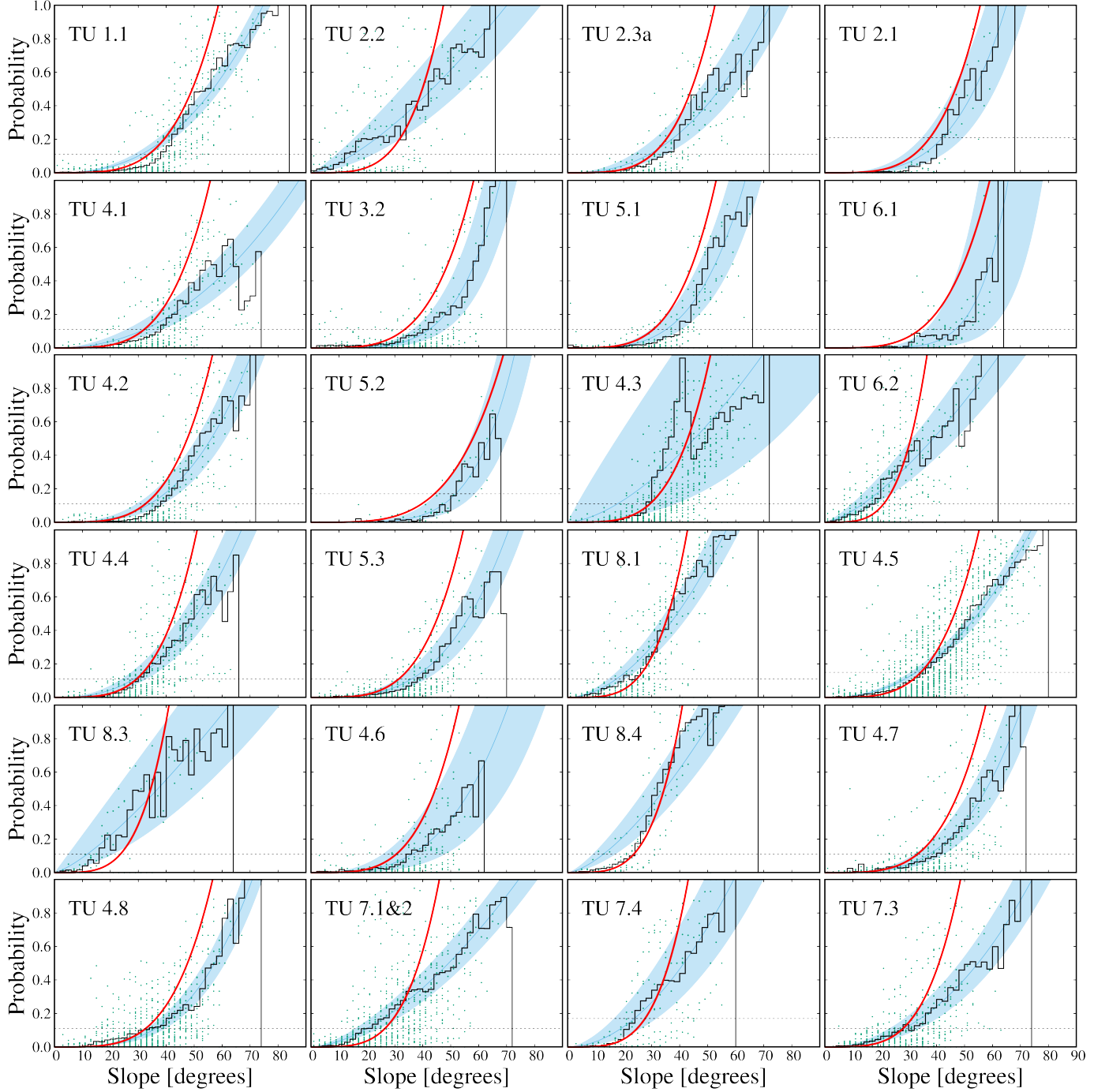


Figure 5: Each panel is as in Fig. 4; topographic unit 1.2 & 1.3 is shown in Fig. 4; 2.3a and 2.3b were grouped into one section, for what concerns modeling of source areas; section 3.1 does not contain mapped sources; sections 6.3 and 8.2 contain no intersections between railway and slope units; this figure shows results for the remaining 24 sections.

grids. Second, using ECDFs makes results independent from the absolute values of the number of simulated trajectories per source grid cell and makes only relative values relevant, consistently with our method of assigning these numbers (*cf. Section 4.1*). We performed the counter-to-relative probability conversion operation separately in each of the 29 topographic units shown in **Figure 1**. **Figure 6** shows sample ECDFs obtained in four topographic

units.

4.3. Analysis of the railway network within graph theory

The railway track running through Italy can be viewed as a collection of links, *i.e.* portions of track running without intersections from a starting point to an arrival point, and of nodes, *i.e.* a geographical network. the intersections.

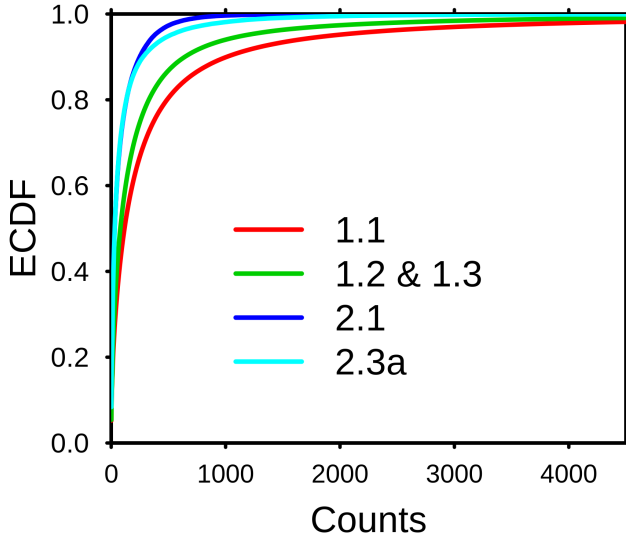


Figure 6: The figure shows sample ECDFs, obtained in four topographic units; (*cf.* Fig 1 and Table 1). We used an approach based on ECDF to map the output of STONE, consisting in a cell-by-cell trajectory count (abscissa), into a relative probability map (ordinate).

Nodes can be connected to multiple links. This collection of links and nodes represents

The links–nodes description can be further assimilated with a graph, whose vertices are the network nodes and whose edges are the network links. We performed a simple preliminary analysis of the graph corresponding to the railway network, calculating betweenness of vertices and edges. This analysis describes the topology of the graph, and it is a starting point for discussing rockfall susceptibility in relation to the railway network operativity. **Figure 7** is a graphical representations of such analysis.

Figure 7 is a graph representation of the geographical network, where vertices are now connected by straight lines – graph edges. In **Fig. 7**, the dots colored with a green-to-red palette represent betweenness of vertices (*cf.* **Section 2.2**), with red corresponding to higher values. The representation of edges is twofold. The color of the edges, quantifies with a yellow-to-red palette, represents betweenness of the edges: more central edges (*i.e.* edges crossed by a larger number of all-to-all shortest paths) have larger betweenness. Thickness of the edges, instead, is proportional to the physical distance between the nodes they connect. Edge betweenness in the (weighted) graph, is known to be one of the most important variables in networks (Barthélémy, 2011), and we used it in the subsequent analysis.

To understand the impact of possible interruptions due to rockfalls on the railway network, from graph theory point of view, we performed two separate analyses. First, we considered the impact on the graph (and, correspondingly, on the real network) of removing edges (*i.e.* railway links, consisting of a variable number of 1-km segments) from

the network, one by one. Second, we considered jointly the classification of the railway segments into susceptibility classes and their role in the equivalent graph as described above.

Removing one edge from the graph, all of the remaining edges (as associated to the residual network) change their values of betweenness by a small amount. For each edge in the graph, we calculated total variation betweenness from the original graph to the graph obtained removing the one edge, and assigned this value as an attribute to the removed edge in the original graph. We looped over the whole set of edges, ending up with a new ranking of edges according to the newly calculated attribute. We used the newly defined quantity as an additional index for a joint classification of railway segments. The joint classification is based both on rockfall susceptibility and on the variation of betweenness index, and we named it network–ranked susceptibility.

4.4. Hardware and software settings

Simulations over a large area with the software STONE were not straightforward. The main limitation is that the software calculates the user-defined number of trajectories in a serial way. Despite each calculation is relatively fast, the large number of trajectories needed for this study would make it impossible to run in a single instance. We adopted a simple strategy to overcome this problem, splitting the study areas in many sub–areas and running several instances of STONE in parallel (*cf.* **Section 4.2**). This is allowed, in general, by the fact that the trajectory count output of STONE is additive; thus, the user only has to take care of summing the partial results in overlapping sub–areas. In this work, in particular, we selected groups of contiguous slope units as sub–areas, which ensures that trajectories are bound within each sub–area.

Raster grids were prepared for each sub–area in automatic way within GRASS GIS (Neteler and Mitasova, 2007; Casagrande et al., 2007). We used a multi–core machine, equipped with 48 computing cores and 330 GB RAM memory, to perform in parallel the GIS operations necessary to prepare the grids (*cf.* point 2b, **Section 4.2**), execution of the program itself (*cf.* point 3b) and collection of the 921 sub–results (*cf.* point 4b). The total running time for completing the operations in points 2b, 3b and 4b was about two days, using simultaneously all of the 48 computing cores which run the sub–areas in a master–slave strategy, which best balanced workload. The entire run was repeated a few times, during which a few bugs were fixed, to obtain the final result.

5. Results

This section describes the results the physically based model STONE (Guzzetti et al., 2002) along the national railway network in Italy. We performed simulations in areas encompassed by all of the slope units (Alvioli et al.,

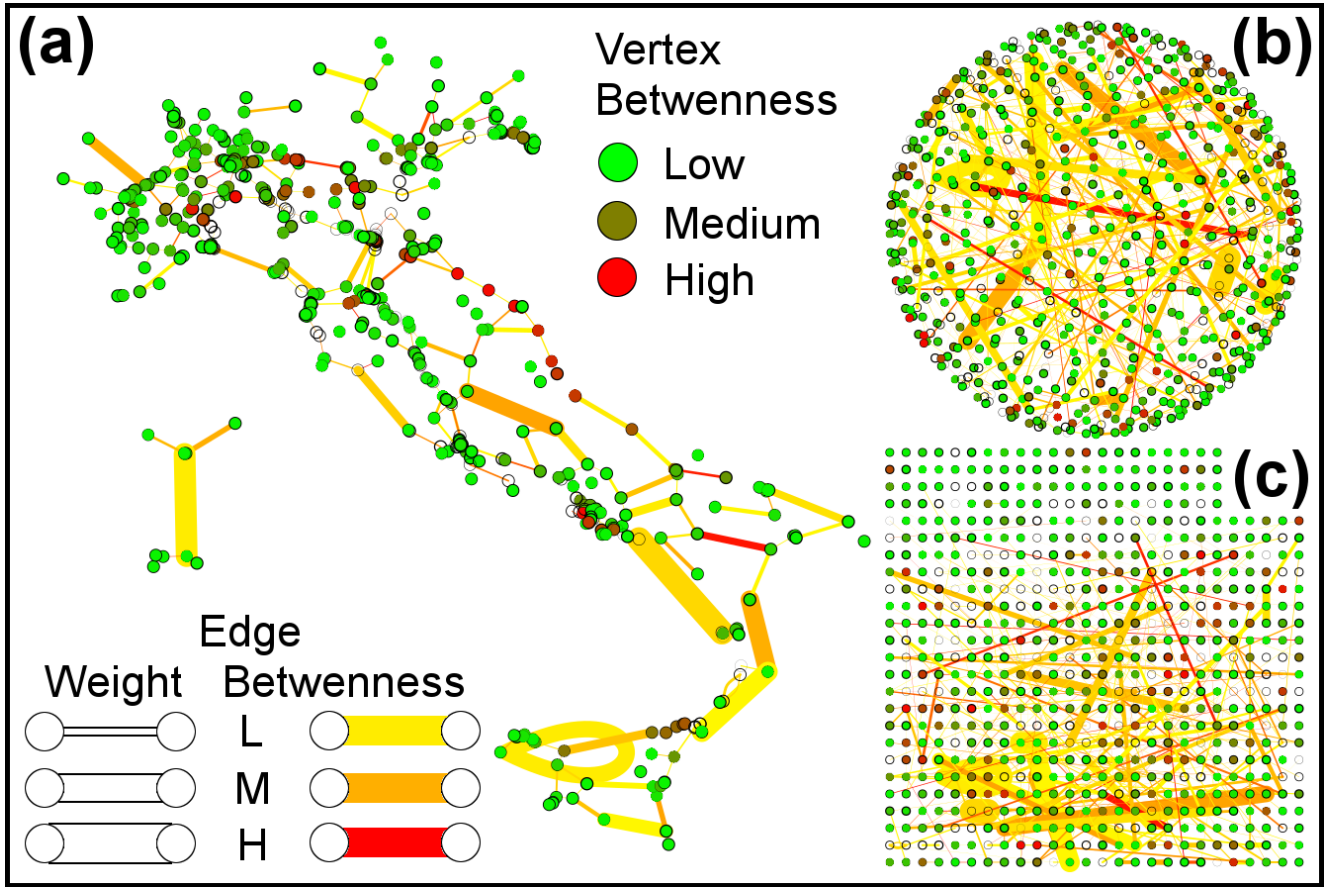


Figure 7: Graphs associated to the railway network. (a) Spatial distribution of vertices (circles) is consistent with their geographical location, and links of the network are represented as straight lines (edges) connecting vertices. (b)-(c) Two alternative representations of the same graph; graphical representations of a graph are infinite, in principle, and a specific one may help highlighting peculiar aspects. In (b), nodes are uniformly distributed on the surface of a sphere; in (c), nodes are on a square grid, showing that most of the nodes are rather peripheral. All of the graphs contains three quantitative measures: (i) color of the vertices, displayed with a green-to-red palette, represents betweenness; (ii) color of the edges, displayed with a yellow-to-red palette, represents the edge betweenness; (iii) thickness of each edge is proportional to the actual (spatial) distance between the two vertices (nodes) it connects. Information content is the same in the three representations.

2016, 2020a) overlapping with a 1 km buffer delineated around the railway track.

Results are described in three different steps:

- (i) agreement between modeled and observed rockfall source areas mapped by experts, and with sub-areas of the polygons in the IFFI inventory (*cf. Section 4.1*);
- (ii) assessment of the trajectory count output of the program STONE, performed calculating the agreement between runout areas and polygons in the IFFI inventory; classification of railway segments into rockfall susceptibility classes (*cf. Section 4.2*);
- (iii) analysis of the impact of the network classification for the railway network within the newly defined network-ranked susceptibility (*cf. Section 4.3*).

We believe it interesting to show and discuss separately the results of source area modeling, point (i), since they represent a relevant input to the physically based model used

in this work and, probably, to similar approaches. The procedure we developed for the purpose was calibrated on a sample of expert-mapped source areas. The output of the statistical generalization is a grid with probabilistic interpretation; comparison between modeled probability and mapped source areas used for calibration, thus, is meaningful. To this end, we calculated the number of grid cells encompassed by polygons representing mapped source areas in which the statistical procedure assigned non-null probability, and the number of cells with values of probability larger than 0.8, to check if larger probabilities are found within the mapped polygons.

Relevance of point (ii) is straightforward, as rockfall susceptibility along the railway track is the primary goal of this work. Point (iii) gives insight into the mutual relationship susceptibility classes and the role of each railway segment within the network as a whole.

5.1. Results of the procedure to identify source areas

The procedure described in **Section 4.1** applies to each of the topographic units adopted in this work. **Figure 4** and **Fig. 5** illustrate the probability–slope dependence; **Table 3** lists, for each topographic unit: the total area, the area of slope units considered in this work (*i.e.*, the extent of the study area), the number and total area of the expert–mapped polygons of potential source grid cells.

For illustrative purposes, due to the large extent of the study area, we show details of expert mapping and source selection procedure, and their comparison, for one specific topographic unit, namely unit 1.2 & 1.3 (Central-Eastern Alps & Carso) of Guzzetti and Reichenbach (1994). **Figure 8(a)** shows an overall view of unit 1.2 & 1.3, the railway track, the polygons mapped by experts in this unit, along with the portion of IFFI rockfalls overlapping with the set of SUs in this unit. Similar settings were found across the whole study area, about 25,000 km².

In **Fig 8(b)**, the detail shows a zoom of a few slope units in the north–east of the unit, in which both expert-mapped and IFFI polygons are present (small blue box in the top figure). IFFI polygons are split into main body (purple pattern), their portion below the 10th elevation percentile (“IFFI Lo”, cyan) and the portion above 90th elevation percentile (“IFFI Hi”, green). Percentiles help showing that most IFFI rockfall polygons actually contain both the source, runout and deposition zone. We infer that from the fact that the upper percentile lies on top of slope units and approximately corresponds with expert–mapped sources, while the lower percentile lies at the bottom of slopes and stretches down to the valley, for the larger polygons. These characteristics were shared by all of the IFFI rockfall polygons that we explicitly checked visually. We use upper and lower percentiles to have a general overview of the performance of both source selection and simulation results, in the following.

The output of the generalization is a 10 m x 10 m grid map aligned with the TINITALY DEM, whose value in each cell is the probability for a rockfall trajectory to originate from that specific location. An example probabilistic source map selected within topographic unit 1.2 & 1.3 is in **Fig. 9(a)**

A comparison between modeled probability and expert–mapped source areas represents an evaluation of the performance of the calibration step of the source identification procedure. Performance is quantified by hit rate of modeled probability versus truth, represented by mapped polygons. We considered the modeled probability in two different ways. We either selected all of the grid cells for which the statistical procedure assigned any non-null probability, and cells with values of probability larger than 0.8, as an arbitrary threshold to distinguish values of “high” probability.

We devised a second comparison, using rockfall polygons

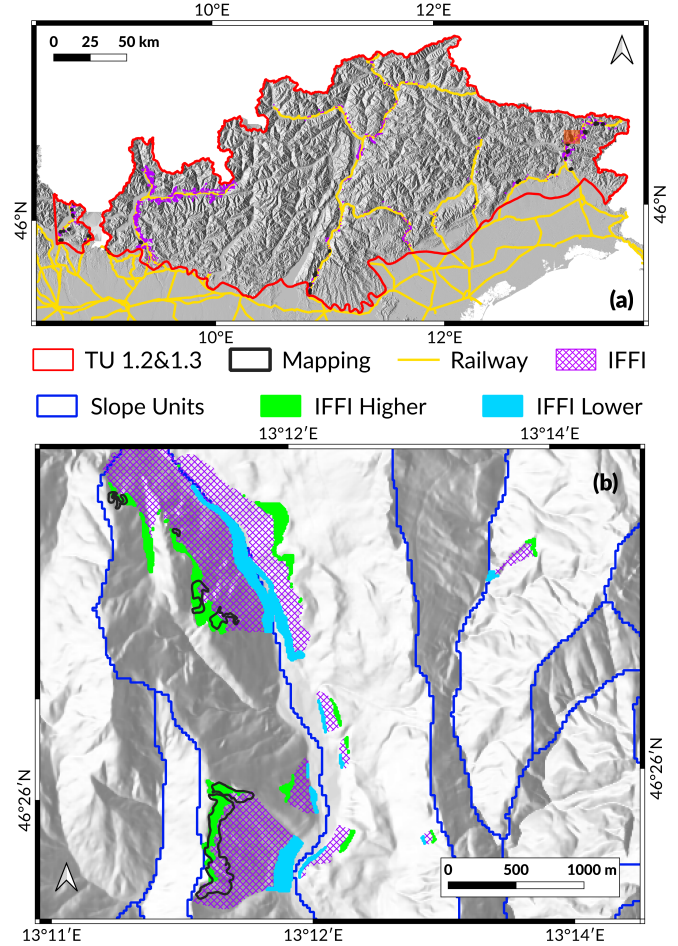


Figure 8: The relationship between expert–mapped source area and the IFFI inventory, limited to the buffer around the railroad track. (a) Overall view of one topographic unit. (b) A detail (small orange in the top figure) showing a few slope units in which both expert–mapped areas and IFFI polygons are present; one can see that, in this case, expert–mapped areas approximately agree with the 90th elevation percentile of IFFI polygons, and that the 10th elevation percentile of the polygons extends down to the bottom of the valley.

in the IFFI inventory (Trigila et al., 2010), intended as a validation step of the procedure for source identification. We calculated, within each polygon in the inventory, the portion corresponding to the upper 90% in elevation. This was our best (arbitrary) guess to what could have been the source area of each catalogued rockfall.

Results for the comparisons in each of the topographic units are listed in **Table 3**. We evaluated the degree of match between model and truth (mapped areas) by hit rate, defined as $HR = TP/(TP + FN)$, where TP stands for true positives and FN for false negatives. Given that $TP + FN = P$, the total attempts of making a prediction (we do not consider negatives, here), the index gives a measure of the percentage of times a prediction was a hit, out of the total attempts. We did not evaluate its counterpart, true negative rate, or a full confusion matrix: true negatives are unknown, here, because we did not know if IFFI

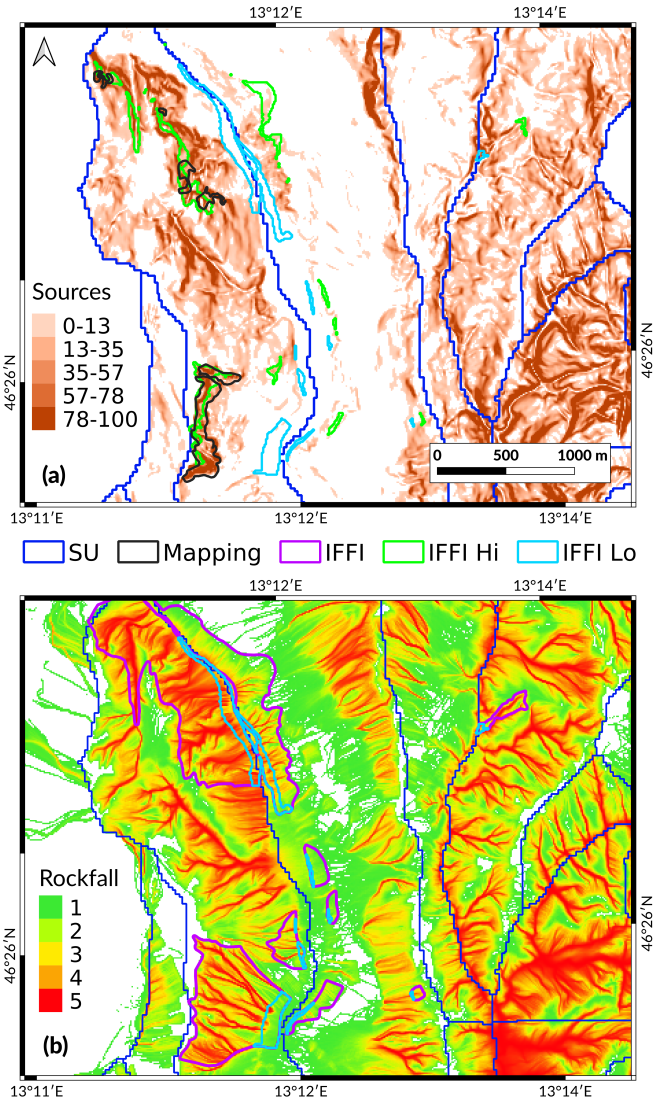


Figure 9: (a) Modeled source areas (classified in shades of brown) and their relationship with expert-mapped source areas (black) and different elevation percentiles of IFFI polygons. (b) Modeled rockfall trajectory count (classified with a green-to-red color ramp) and its relationship with whole IFFI polygons (purple) and their 10th elevation percentile (cyan).

is a complete inventory. Hit rate was calculated within the slope units selected as study area for this work.

Table 3 shows HR corresponding to four combinations of HR calculated as: (i) modeled sources, with any probability value, against the expert-mapped source areas (“Mapped Total”); (ii) modeled sources, limited to cells with highest probability, against the expert-mapped source areas (“Mapped $P > 80\%$ ”); (iii) modeled sources, with any probability value, against the upper 90% elevation of IFFI polygons (“IFFI Total”); (iv) modeled sources, with highest probability, against the upper 90% elevation of IFFI polygons (“IFFI $P > 80\%$ ”).

Combination (i): HR between modeled sources (cells assigned with non-null probability of being a source) and

expert-mapped source areas is below 75% in 12 topographic units, namely: 2.2 (Veneto Plain), 3.1 (Monferrato Hills), 4.6 (Sila), 4.7 (Aspromonte), 4.8 (Sicilian Apennines), 5.1 (Tyrrhenian Borderland), 7.1 & 7.2 (Marsala Lowland & Sicilian Hills), 7.3 (Iblei Plateau), 8.1 (Sardinian Hills) and 8.3 (Campidano Plain). Out of the 12 sections, five are below 50%, of which two (units 2.2 and 3.1) are below 25%. The corresponding sections have small or very small total SU area, and many are located in the vicinities of plains or coasts, which are probably the most difficult to model on a regional or national level as they differ the most from the typical settings in which we mapped sources in expert way.

Combination (ii): the validity of this comparison is probably more difficult to understand on general grounds. Out of the 26 sections (three out of the original 29 were ruled out by absence of railway track or absence of slopes prone to rockfalls), four have HR larger than 20%, 11 sections show smaller than 10%, five of them smaller than 5%.

Combination (iii): HR results of the comparison between modeled sources and polygons labeled as “rockfall” or “extended areas containing rockfalls” in the IFFI national inventory. In this case, compared with the region above the 90th elevation percentile, within each polygon. Results reveal a lower degree of match with respect to case (i): 20 sections assigned with HR less than 75%, of which 13 smaller than 50%, of which one smaller than 25%.

Combination (iv): as in case (ii), interpretation of the comparison is less obvious than the one with any value of probability for mapped sources, case (iii). Out of the 26 relevant sections, one has HR larger than 20%, 13 sections show HR smaller than 10%, five of them smaller than 5%.

5.2. Results for rockfall susceptibility within the model STONE

The final product of this work is a classification of the railway track in Italy, split into 1-km segments, with susceptibility values for the occurrence of rockfalls. To this end, the most relevant points are as follows (*cf.* enumerated list in Section 4.2). We prepared maps of trajectory count per cell using the model STONE. Then, we classified all of the cells encompassed by the selected SUs (*cf.* step 2a of the enumerated list in Section 4.1); we used the map to calculate a unique value of susceptibility per 1-km segment of the track.

We converted the trajectory count map, containing wildly varying values, into the [0,1] interval – consistent with a (relative) probability, *i.e.* susceptibility. We did so using ECDF functions calibrated in the subset of grid cells in which rockfalls are known to have occurred, reported in the national IFFI inventory (Trigila et al., 2010). The inventory contains polygons mapped as “rockfalls” or as

Table 4: Hit rate for the validation of rockfall runout areas, *i.e.* obtained from the comparison of probability of occurrence P_{QR} from reclassification of trajectory count map by means of ECDFs as described in **Section 4**. The ID in the first column corresponds to topographic units of **Fig. 1**, **Table 1** and **Table 3**. “Total” HR values correspond to values of any non-null probability value, and partial HR values to probability between the specified intervals. The largest value among the partial ones is in bold. This comparison involves only the 10th elevation percentile of each polygon in the IFFI inventory.

| Section ID | HR (Total) | HR [0,0.2) | HR [0.2,0.4) | HR [0.4,0.6) | HR [0.6,0.8) | HR [0.8,1.0] |
|------------|---------------|---------------|-----------------|-----------------|-----------------|-----------------|
| 1.1 | 95% | 33% | 19% | 17% | 13% | 13% |
| 1.2 & 1.3 | 95% | 19% | 16% | 19% | 20% | 22% |
| 2.1 | 100% | 3% | 14% | 22% | 19% | 41% |
| 2.2 | 98% | 3% | 4% | 18% | 27% | 46% |
| 2.3a | 96% | 13% | 12% | 20% | 23% | 29% |
| 2.3b | — | — | — | — | — | — |
| 3.1 | 2% | 0% | 0% | 0% | 1% | 1% |
| 3.2 | 74% | 23% | 14% | 12% | 10% | 15% |
| 4.1 | 91% | 13% | 11% | 21% | 22% | 23% |
| 4.2 | 81% | 16% | 13% | 5% | 25% | 22% |
| 4.3 | 96% | 37% | 15% | 9% | 21% | 14% |
| 4.4 | 85% | 15% | 10% | 10% | 17% | 33% |
| 4.5 | 97% | 9% | 8% | 11% | 19% | 49% |
| 4.6 | 60% | 13% | 8% | 12% | 11% | 16% |
| 4.7 | 75% | 14% | 15% | 18% | 16% | 13% |
| 4.8 | 93% | 13% | 14% | 20% | 22% | 24% |
| 5.1 | 71% | 33% | 20% | 14% | 3% | 2% |
| 5.2 | 43% | 8% | 7% | 5% | 5% | 18% |
| 5.3 | 79% | 21% | 15% | 12% | 15% | 16% |
| 6.1 | 59% | 14% | 10% | 14% | 14% | 6% |
| 6.2 | 85% | 52% | 14% | 7% | 10% | 3% |
| 6.3 | — | — | — | — | — | — |
| 7.1 & 7.2 | 76% | 16% | 13% | 13% | 19% | 15% |
| 7.3 | 77% | 9% | 12% | 9% | 11% | 35% |
| 7.4 | 8% | 3% | 2% | 1% | 1% | 1% |
| 8.1 | 52% | 13% | 9% | 9% | 11% | 11% |
| 8.2 | — | — | — | — | — | — |
| 8.3 | 81% | 17% | 17% | 9% | 21% | 17% |
| 8.4 | 97% | 38% | 28% | 11% | 8% | 12% |

“extended areas containing rockfalls”. We calculated specific ECDFs in each topographic unit shown in **Fig. 1**. **Figure 6** shows a few sample ECDFs corresponding to the first four topographic units in **Tables 3, 4** and **5**. The remaining ECDFs are very similar, and curves would overlap with those in **Fig. 6**.

Figure 9(b) shows the final, classified trajectory count (susceptibility) in a sample location. The raster map is colored with a green-to-red color ramp from low to high values of susceptibility. In the figure, we compare the susceptibility map with the IFFI polygons existing in the area (*cf.* **Fig. 8**). We performed validation of the classified output in the susceptibility map as follows. We selected all of the rockfall polygons from the IFFI inventory within the slope units buffer, and further selected the DEM grid cells under the polygons and falling in the lowest 10th elevation percentile – also shown in **Fig. 9**. We are reasonably confident that these cells represent rockfall deposit areas.

Comparison of probability maps among different topographic units with deposit areas inferred from IFFI poly-

gons, and with the whole IFFI polygons, provided values of hit rate ($HR = TP/(TP + FN)$) listed in **Table 4** and labeled as “Total” HR . Similarly, we defined “partial” HR values, limiting the calculations within the individual classes delimited by (0, 0.2, 0.4, 0.6, 0.8, 1) values, whose results are also listed in **Table 4** in five additional columns.

Table 5 has a similar structure as **Table 4**, but it lists results corresponding to comparison of modeled source areas with the whole extent of rockfall polygons in the IFFI inventory. Topographic unit 2.3b does not contain rockfalls recorded in the IFFI inventory relevant to the railway track, while sections 6.3 and 8.2 do not contain intersections of the track with slope units. Thus, we reported no values for such zones in **Tables 4 and 5**.

The next step was the classification of the railway network split into 1-km segments and classified using a simple strategy. For each segment, overlapping many susceptibility values we selected the largest value. This is a conservative and reasonable choice, given that if a single point of the segment would be hit by a rockfall, the whole segment

Table 5: As in Table 4, but the comparison involves whole polygons in the IFFI inventory.

| Section ID | HR (Total) | HR [0,0.2) | HR [0.2,0.4) | HR [0.4,0.6) | HR [0.6,0.8) | HR [0.8,1.0] |
|----------------------|---------------|---------------|-----------------|-----------------|-----------------|-----------------|
| 1.1 | 97% | 19% | 22% | 20% | 18% | 18% |
| 1.2 & 1.3 | 95% | 17% | 19% | 19% | 19% | 20% |
| 2.1 | 95% | 13% | 13% | 14% | 22% | 33% |
| 2.2 | 93% | 16% | 18% | 21% | 20% | 18% |
| 2.3a | 93% | 18% | 19% | 19% | 19% | 19% |
| 2.3b | — | — | — | — | — | — |
| 3.1 | 6% | 1% | 1% | 0% | 2% | 1% |
| 3.2 | 60% | 12% | 13% | 12% | 12% | 12% |
| 4.1 | 90% | 12% | 15% | 17% | 21% | 24% |
| 4.2 | 84% | 24% | 16% | 15% | 18% | 12% |
| 4.3 | 95% | 16% | 19% | 20% | 20% | 20% |
| 4.4 | 81% | 14% | 16% | 17% | 17% | 17% |
| 4.5 | 94% | 17% | 19% | 19% | 19% | 19% |
| 4.6 | 65% | 12% | 13% | 13% | 13% | 13% |
| 4.7 | 72% | 13% | 16% | 16% | 15% | 13% |
| 4.8 | 80% | 15% | 16% | 16% | 17% | 17% |
| 5.1 | 58% | 24% | 19% | 10% | 4% | 1% |
| 5.2 | 36% | 9% | 6% | 5% | 7% | 9% |
| 5.3 | 89% | 17% | 18% | 18% | 18% | 18% |
| 6.1 | 65% | 10% | 11% | 14% | 15% | 15% |
| 6.2 | 78% | 16% | 15% | 16% | 16% | 16% |
| 6.3 | — | — | — | — | — | — |
| 7.1 & 7.2 | 55% | 12% | 12% | 12% | 11% | 9% |
| 7.3 | 83% | 10% | 15% | 19% | 20% | 20% |
| 7.4 | % | % | % | % | % | % |
| 8.1 | 40% | 8% | 8% | 8% | 8% | 8% |
| 8.2 | — | — | — | — | — | — |
| 8.3 | 82% | 17% | 17% | 17% | 19% | 12% |
| 8.4 | 87% | 15% | 17% | 17% | 19% | 19% |

would be unusable. On the other hand, splitting the whole link connecting two nodes into small segments of the same length guarantees spatial homogeneity. **Figure 10** shows the railway segments classified as outlined above. Out of the total 16,084 km of railway track (the track length is less than the total, above 17,000 km, due to tunnels and a few areas outside of the TINITALY), 14,724 km were classified in [0,0.2), 239 km in [0.2,0.4), 170 km in [0.4,0.6), 163 km in [0.6,0.8) and 789 km in [0.8,1.0].

Unfortunately, available data was insufficient to perform a validation of the result of the classification of segments. To perform an additional assessment of the results, we performed graph analysis, and evaluated its implications for the operativity of the railway network.

5.3. Impact of rockfalls on the railway network: network-ranked susceptibility

In **Section 4.3** we described an analysis of the railway network in terms of graph theory. We defined a new index for each railway segment, obtained as the variation of total edge betweenness on the network if the edge corresponding to the segment is removed from the graph. **Figure 11** shows the result of the analysis; edges are colored with a white-to-blue color palette, for increasing value of the

attribute calculated by removing one edge at a time. The figure clearly highlights the most relevant edges, topology-wise, and one can easily spot the difference between this analysis and edge betweenness, **Fig. 7**.

The result of **Fig. 11** is an intermediate step towards the definition of a combined quantity, defined considering simultaneously the variation of betweenness, thus strictly related to network properties, and classification of the railroad based on rockfall susceptibility. The combination was performed in the simplest possible way, by crossing the classes of both quantities to obtain a new classification, the last result of this work.

Classes based on rockfall susceptibility of railway links, split in 1-km segments, was defined in **Section 4.2**, and **Fig. 10** shows the results. Variation of betweenness on removal of one graph edge was defined in this section, and it is shown in **Fig. 11**. Here, we classify the latter quantity into five classes using the head/tail breaks method (Jiang, 2013). Natural breaks is a standard classification method, though seldom used, which in our case allowed to classify our sample in a more meaningful way with respect to more common methods. It simply works by calculating the average value of the quantity of interest, split the sample into values below and above the average, then select the

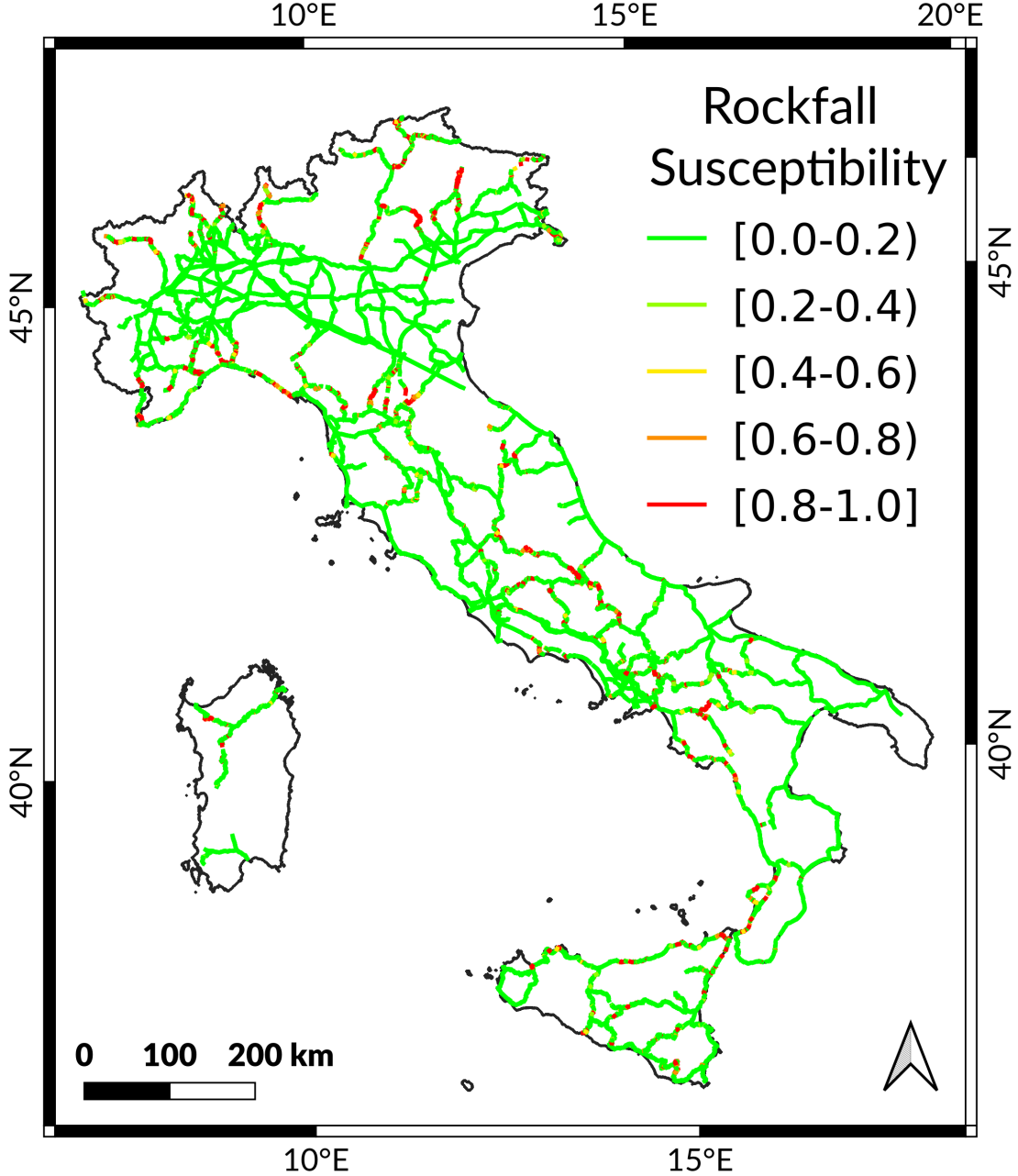


Figure 10: Classification of the railway network, split into segments of 1 km length, with the procedure developed in this work. Segments are colored with a red-to-green palette, corresponding to low-to-high susceptibility for rockfalls.

more numerous split and repeat the procedure, until five classes are obtained.

We refer to the joint classification of susceptibility and segment relevance as network-ranked susceptibility. Results for network-ranked susceptibility, expressed in terms of kilometers or railway in each class, are in **Table 6**. The table clearly shows the classification obtained by crossing five classes in the two considered attributes, *i.e.* segment relevance (score) and rockfall susceptibility. The 25 classes are further colored (*i.e.*, further classified) using seven colors, in order of increasing ranked susceptibility:

white, light green, deep green, yellow, deep yellow, orange, red. We defined the coloring scheme in a totally arbitrary way, except that: (i) the lowest rockfall susceptibility class, corresponding to the largest portion of railroad, was split into two classes of network-ranked susceptibility, and (ii) the remaining portion of the railroad was (almost) evenly distributed into additional five classes. We applied the same coloring scheme of **Table 6** to the graphical representation of the classification of segments, **Fig. 12**. Comparison with the results of classification based on the only susceptibility highlights manifest differences. In fact, while reddish segments are consistently located in

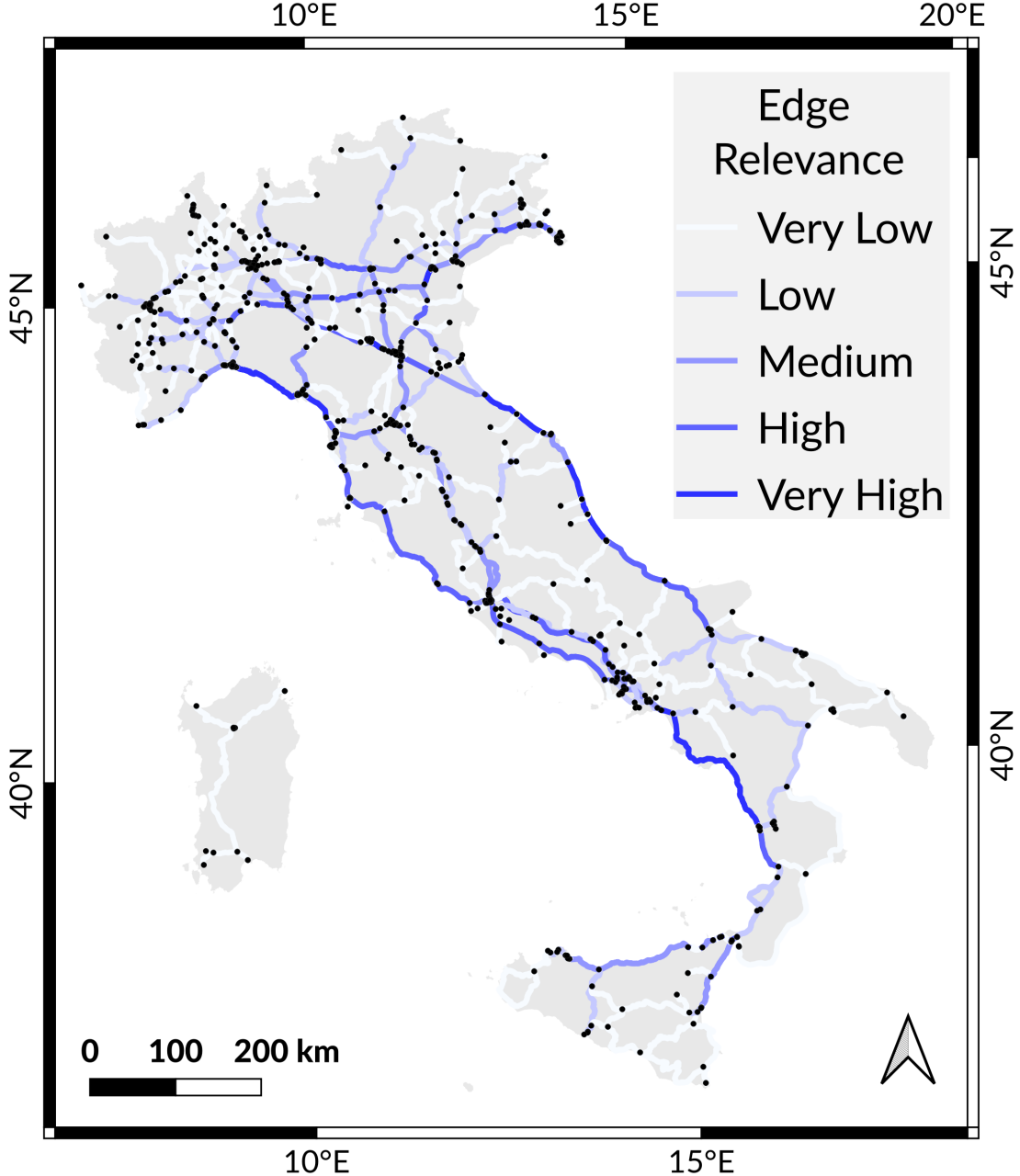


Figure 11: A measure of relevance of railway links in the Italian railway network, alternative to betweenness. Relevance is shown with a white-to-blue color palette; blue denotes more relevance. Relevance is high if total variation of vertex betweenness is high, when the corresponding edge is removed from the graph (*cf. Fig. 7*).

hilly and mountainous areas, plain areas now contains the “very low” and “low” classes of network-ranked susceptibility, while they just had the lowest class of susceptibility; this was a totally arbitrary choice. We discuss the possibility of optimizing the new network-ranked susceptibility in the next section.

6. Discussion

As for the Methods and Results sections, we discuss separately the source areas identification procedure, rockfall

susceptibility assessment and implications from network analysis combined with susceptibility.

We stress here that we used the national landslide inventory IFFI (Trigila et al., 2010; ISPRA, 2018) in several ways. In fact, we calculated hit rates of the statistical generalization of expert-mapped source areas and hit rates of runout areas against proper subsets and sub-areas of the polygons in the IFFI inventory. Nevertheless, we did not actually use the inventory for building or calibrating the rockfall model adopted here.

6.1. Identification of rockfall source areas

An illustration of the comparison between modeled source probability, expert-mapping sources and the upper elevation percentile of IFFI polygons is in **Fig. 9**, for one particular region in topographic unit 1.2 & 1.3. We can see that in this region non-null pixels of the probabilistic source map have a wider extent than both expert-mapping and IFFI upper elevation percentile. This is by construction, because the statistical procedure described in **Section 4.1** was devised to conservatively assign non-null probabilities to any grid cell, based on their slope. This is consistent with the observation that expert-mapped sources actually contain low values of slopes (*cf. Figs. 4 and 5*). **Figure 9(a)** shows a nice agreement between dark-shaded probabilistic map and both IFFI upper elevation percentile and expert-mapped area, though not all areas match perfectly.

Nevertheless, values of model match against the mapped and IFFI polygons, in **Table 3** are often rather low. We attribute that to the following reasons. To build a model of source areas, we hypothesized a relationship between the probability of a grid cell of initiating a rockfall and local slope. This represents a compromise between an acceptable overall time needed for the procedure over a large study area and a realistic product, but it certainly does not embed all of the local terrain properties that influence the expert criteria applied for mapping potential source areas. Moreover, we made specific choices and assumptions, often arbitrary, in the modeling process.

Errors may also arise from the discrepancy between the DEM used in the analysis and the apparent resolution of Google Earth™ imagery used for expert mapping, especially in the locations with steepest relief, the ones in which we are mostly interested in. In the analysis, we used a DEM generated from a triangulated irregular network (TIN); visual inspection of a shaded relief generated from the DEM highlighted locations in which the triangulation used to prepare the DEM is manifest, which surely affects the slope map, nation-wide.

6.2. The model STONE and rockfall susceptibility

The output of the model STONE is a raster map: the classified trajectory count per grid cell. We used it in several ways, to get to the final results of this work: (i) we compared the classified output with the relevant subset of the IFFI inventory; (ii) we split the railway network into 1-km segments and classified them on the basis of rockfall susceptibility; (iii) we studied the properties of the railway network within graph theory, considering the network in relation with the susceptibility results, which helped defining a joint classification.

Tables 4 and **5** list results of the validation against IFFI polygons. Values for the total hit rate in this case are rather large, which means that most of the runout areas in the inventory were actually overlapping with at least one

trajectory. Considering the “partial” HR in **Table 4**, we find that in most cases runout areas (maxima thereof, in bold) fall within the [0.8,1.0] susceptibility class, many fall within the [0,0.2), a few within the [0.4,0.6) and [0.6,0.8) classes, while there are none in the [0.2,0.4) class. This information does not call for straightforward conclusions, though it might be interesting for future reference if an update of the methods presented in this work will be implemented. This could most probably be in the procedure for the selection of source areas (for example as suggested at the end of **Section 6.2**, or as in Rossi et al. (2021)), or in the strategy for classification of the trajectory count.

Results in **Table 5** correspond to validation against the whole extent of polygons in the IFFI inventory, at variance with **Table 4**. Values of “Total” hit rate are rather similar to the case where we compared to the 10th elevation percentile of each polygon, in a few cases a slightly higher. Interestingly, in this case, values of hit rates are almost always equally distributed among the five sub-classes of probability. One reason for that could be due to spatial inaccuracies of the polygons in the inventory.

6.3. Network-ranked rockfall susceptibility

Network-ranked susceptibility for rockfalls, shown in **Table 6** and **Fig. 12**, was defined in this work as a straightforward combination of five classes in edge ranking and rockfall susceptibility. We already noted that the proposed classes produce somewhat striking results, **Fig. 12**, in that segments with negligible rockfall susceptibility (*cf. Fig 10*) do not fall in the lowest class of network-ranked susceptibility. We stress that the seven classes (colors) shown in **Table 6** were chosen almost arbitrarily – hence the apparent mismatch. We consider the classification proposed here as a methodological proposal, and we did not attempt a higher-level optimization of final classes, which we could actually perform with suitable validation data.

Validation of susceptibility requires accurate data about observed rockfall occurrences, possibly including information about whether rockfalls did or did not cross the railway track. Calibration and validation of network-ranked susceptibility, in addition, would require information about the actual operation of the network. A calibration/validation procedure for network-ranked susceptibility, provided data is available, could rely on the application of multi-criteria decision making (MCDM) and optimization methods (Velasquez and Hester, 2013).

Knowledge of actual traffic on the railroad would imply different network properties. In fact, betweenness of nodes and edges was calculated here considering all-to-all shortest paths. If we replaced them with actual routes we would obtain a different network and corresponding graph (Kurant and Thiran, 2006a). As another example, knowledge of the number of trains running on each railroad link per

Table 6: Table shows the cross-comparison of rockfall susceptibility (increasing from left to right) *vs.* segment relevance (score, increasing from top down; classes are as follow: S1, 0–687; S2, 688–3006; S3, 3007–9014; S4, 9015–32914; S5, 329515–512079), each distinguished in five classes as described in **Section 5**. The different colors define a joint classification, named network-ranked susceptibility: white, very low (VL); light green, low (Lo); dark green, medium-low (ML); yellow, medium (Me); light orange, medium-high (MH); dark orange, high (Hi); red, very high (VH). Values are in kilometers; total length (16,084 km) is shorter than the whole railway network because we removed tunnels and segments (few kilometers) laying outside the TINITALY DEM. Segments on plain topography (*i.e.*, non overlapping with slope units) are included, here.

| | | Rockfall Susceptibility | | | | | Sum |
|-----------------------|-----|-------------------------|---------|---------|---------|---------|--------|
| | | 0.0–0.2 | 0.2–0.4 | 0.4–0.6 | 0.6–0.8 | 0.8–1.0 | |
| Railway Segment Score | S1 | 1,432 | 16 | 11 | 10 | 42 | 1,511 |
| | S2 | 782 | 11 | 5 | 7 | 21 | 826 |
| | S3 | 2,506 | 52 | 33 | 33 | 188 | 2,811 |
| | S4 | 4,655 | 86 | 67 | 64 | 323 | 5,195 |
| | S5 | 5,348 | 73 | 54 | 50 | 215 | 5,740 |
| | Sum | 14,724 | 239 | 170 | 163 | 789 | 16,084 |

day could be used to define relevance of edges in a different way, beyond the simple topology of the network considered here. Additional information on the average number of passengers per link/day could help in a similar way. On the other hand, knowledge of real time presence of trains of each link of the network, though not difficult to consider in technical terms, is not immediately relevant for this work. That would require inclusion of some dynamical mechanism for the actual detachment of rocks uphill from each railway link, along with real time monitoring of possible triggering events; for example, rainfall (Rossi et al., 2012) and/or seismic activity (Tanyaş et al., 2019a,b).

7. Conclusions

We described a comprehensive modeling chain for the assessment of rockfall susceptibility along the railway network in Italy. To cope with issues related with the large size of the study area, extensive mapping and computational challenges, we necessarily adopted assumptions and approximations. These were discussed in details throughout this work, in which we described the performance of the different steps of the procedure and we highlighted weak points and possible improvements. An additional point to stress here is that, due to the large size of the study area and unavailability of specific data, rockfalls on anthropic slopes were not considered. On the other hand, we highlighted the merits of this work as an effective procedure for rockfall susceptibility assessment over a very large and geomorphologically diverse study area.

We described three main steps: (i) localization of rockfall source areas on a digital landscape, with different probabilities, (ii) simulation of rockfall trajectories stemming from any possible source area, and (iii) assessment of the impact on the operativity on the railway network as a whole, using a joint classification of network segments taking into account both rockfall susceptibility and network properties. The relevant findings were as follows:

- The procedure for localizing source areas is a statistical generalization of the distribution of slope values within expert-mapped polygons. It was tested in calibration and in validation by comparing results against the original mapped values and against upper-elevation portions of each of the rockfall polygons in the national IFFI inventory. Outcome of the performance assessment, given in terms of hit rate, showed better results in the calibration step, not surprisingly. In general, values of hit rate were seldom in the higher quartile, and mostly in the third and second quartile. Results for the validation were similar. The procedure is suitable for identification of source areas in large areas (here, about 25,000 km²), though improvement of calibration performance would require including additional morphometric variables besides slope. Replication of the procedure in a new or extended area (*i.e.*, the whole of Italy) requires additional expert mapping.
- The modeling procedure of rockfall trajectories, using the program STONE, was validated results against the IFFI inventory again, but using the lowest-

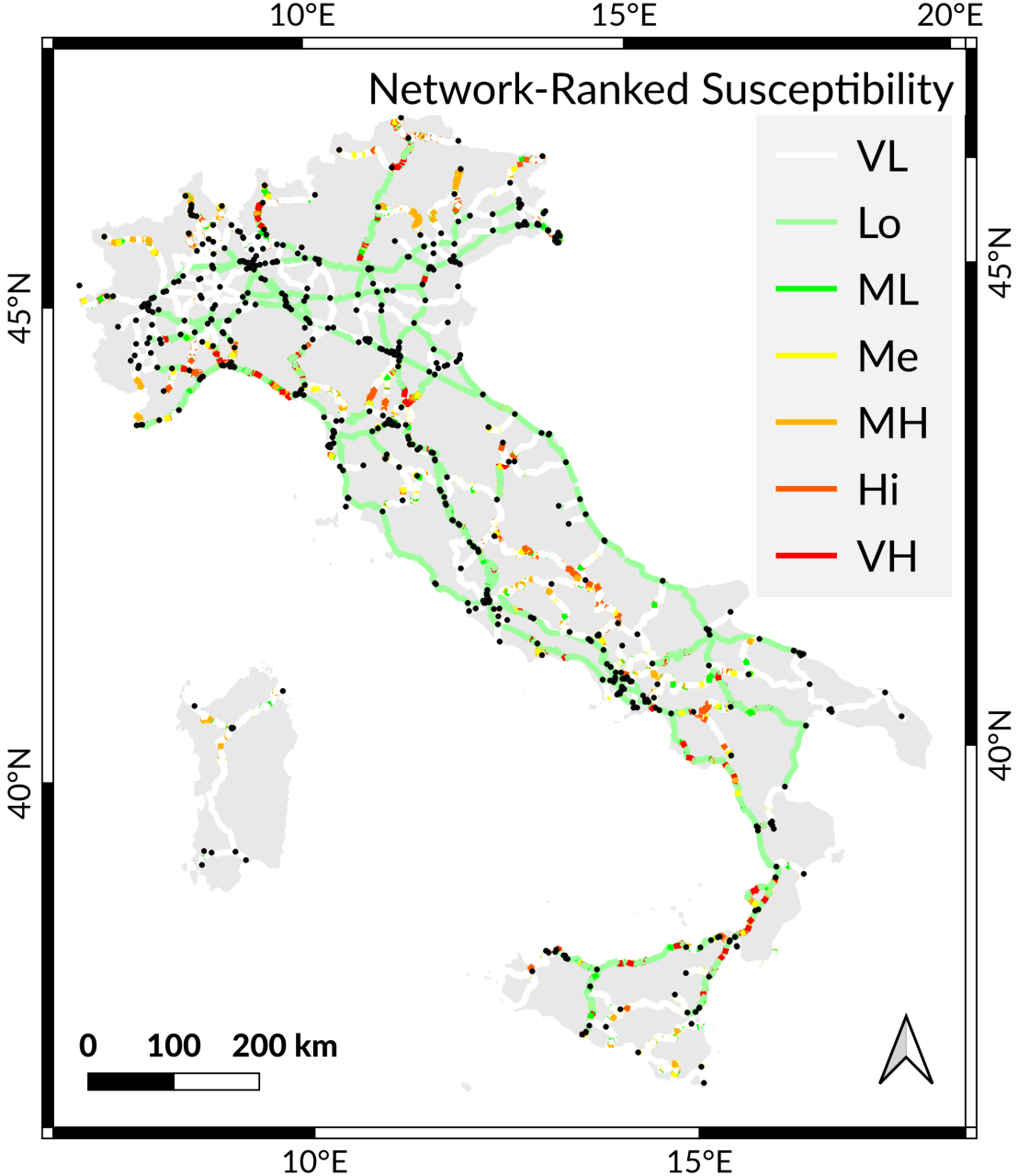


Figure 12: Network-ranked susceptibility, defined as a combination of relevance of railway links, calculated in [Section 4.3](#), and shown in [Fig. 11](#), and segment-wise rockfall susceptibility, modeled in this work with STONE and shown in [Fig. 10](#). [Table 6](#) lists a breakdown of the total railway length, in kilometers, within the seven classes shown in this figure in different colors.

elevation portions of the rockfall polygons, which we assimilated with deposit areas. We compared a classified susceptibility map with so-defined deposits. Findings were that match between the two maps, in terms of hit rate, are rather satisfactory, in that the majority of values were in the higher quartile of the probability distribution. We further cast the susceptibility map onto the railway network, by splitting the railway link in 1-km segments and assigning a class of susceptibility to each segment. Validation of the susceptibility values for segments of the railway requires

additional data, not available to us.

- The analysis possible rockfall impact on the railway considered the effect of the possible disruption of a segment of the railway on the network as a whole, due to a falling boulder. That was quantified by a combination of rockfall susceptibility, as obtained with simulated trajectories within STONE, and a measure of the relevance of each edge of the graph corresponding to the railway network. We defined a new quantity which we called network-ranked susceptibility, considering the joint classification of rockfall susceptibil-

ity and graph properties. We consider this step as a methodological proposal, whose optimization and validation would required dedicated data and additional knowledge of the actual traffic over the railway network.

We stress that, in this work, the national landslide inventory IFFI (Trigila et al., 2010) helped validating results, but did not enter neither in the runout modeling, nor in the identification of sources areas, which required expert source areas mapping. This step of the procedure leaves room for improvement, in that we only used distributions of slope values to characterize expert-mapped polygons. Additional morphometric and thematic variables could be used to improve identification of source areas (e.g., (Rossi et al., 2021)).

Although the most relevant input of the program STONE are the grid cell locations of possible source areas of rockfalls, additional improvements could be implemented in the runout modeling chain. Other numerical inputs of the program could be determined in more appropriate manner than the ones we inferred from the literature, both by means of finer spatial lithological characterization and by considering explicit measurements. The latter can be probably performed only in local applications, in the near future. Moreover, the model STONE does not account for shape and size of falling boulders, nor for their fragmentation; this could be another part in which there is room for improvement. We also noted that the digital elevation model adopted in this work (Tarquini et al., 2007), though very useful for its relatively high resolution, suffers from local inconsistencies and inhomogeneities, due to the aggregation of different data sources and the triangulated irregular network method. Eventually, we stress that source areas, in addition to STONE.

We stress that both steps (identification of source areas and simulation of runout) can, in principle, be extended outside of the buffer considered in this work, because most of the information and methods developed here are still valid. The buffer itself, consisting of slope units overlapping with the railway, can be easily enlarged, given that slope units are available for the whole of Italy (Alvioli et al., 2020a).

Application of ideas from network and graph theory helped finding implications of the different values of rockfall susceptibility along the railway, inferring a network-ranked susceptibility. This part contained both arbitrary and incomplete parts, in that two-fold classification of rockfall susceptibility and relevance of railway links for the operability of the network was performed without any attempt of weighting the twos in different ways, and neglecting actual routes and traffic on the real-world railway. The latter information is unknown to us, and it would be interesting to consider that in a dedicated piece of work.

Eventually, we stress that a natural evolution of the anal-

ysis performed on the topological properties of the railway network is a real-time monitoring (still static, no traffic involved) of the network as a function of the real-time evolution of possible triggering events. This was actually the original motivation of this work. The segment-wise susceptibility map developed in this work, along with analogous map obtained for debris flows susceptibility and soil slides susceptibility are key inputs for the prototype early warning system that was funded by the National railway company (RFI) within the framework for the implementation of the SANF (an acronym for national early warning system for rainfall-induced landslides) system (Rossi et al., 2012; Guzzetti et al., 2020).

8. Acknowledgments

This work was partially supported by RFI gruppo Ferrovie dello Stato Italiane, contract number 488, 01/02/2018.

9. Declaration of competing interests

The authors declare that they have no known competing financial interests or personal relationships that could have appeared to influence the work reported in this manuscript.

References

- Abellán, A., Calvet, J., Vilaplana, J.M., Blanchard, J., 2010. Detection and spatial prediction of rockfalls by means of terrestrial laser scanner monitoring. *Geomorphology* 119, 162–171. doi:10.1016/j.geomorph.2010.03.016.
- Agliardi, F., Crosta, G.B., 2003. High resolution three-dimensional numerical modelling of rockfalls. *International Journal of Rock Mechanics and Mining Sciences* 40, 455 – 471. doi:10.1016/S1365-1609(03)00021-2.
- Ahuja, R.K., Magnanti, T.L., Orlin, J.O., 1993. *Network Flows: Theory, Algorithms, and Applications*. Prentice Hall Inc., Upper Saddle River, New Jersey.
- Albert, R., Jeong, H., Barabási, A.L., 2000. Error and attack tolerance of complex networks. *Nature* 406, 378—382. doi:10.1038/35019019.
- Alvioli, M., 2020. Administrative boundaries and urban areas in Italy: A perspective from scaling laws. *Landscape and Urban Planning* 204, 103906. doi:10.1016/j.landurbplan.2020.103906.
- Alvioli, M., Guzzetti, F., Marchesini, I., 2020a. Parameter-free delineation of slope units and terrain subdivision of Italy. *Geomorphology* 358, 107124. doi:10.1016/j.geomorph.2020.107124.
- Alvioli, M., Marchesini, I., Reichenbach, P., Rossi, M., Ardizzone, F., Fiorucci, F., Guzzetti, F., 2016. Automatic delineation of geomorphological slope units with *r.slopeunits v1.0* and their optimization for landslide susceptibility modeling. *Geoscientific Model Development* 9, 3975–3991. doi:10.5194/gmd-9-3975-2016.
- Alvioli, M., Santangelo, M., Fiorucci, F., Cardinali, M., Marchesini, I., Reichenbach, P., Rossi, M., 2020b. A data-driven method for assessing the probability for terrain grid cells of initiating rockfalls on a large area, in: Alvioli, M., Marchesini, I., Melelli, L., Guth, P. (Eds.), *Proceedings of the sixth Geomorphometry conference: Geomorphometry 2020*, CNR Edizioni, Rome, Perugia, Italy. doi:10.30437/geomorphometry2020_43.
- Amato, G., Fiorucci, M., Martino, S., Lombardo, L., Palombi, L., 2020. Earthquake-triggered landslide susceptibility in Italy by means of artificial neural network. [Https://doi.org/10.31223/X59W39](https://doi.org/10.31223/X59W39).

Barthélemy, M., 2011. Spatial networks. *Physics Reports* 499, 1–101. doi:10.1016/j.physrep.2010.11.002.

Bassolas, A., Gallotti, R., Lamanna, F., Lenormand, M., Ramasco, J.J., 2020. Scaling in the recovery of urban transportation systems from massive events. *Scientific Reports* 10, 2746. doi:10.1038/s41598-020-59576-1.

Battaglini, L., Campo, V., Cipolloni, C., Congi, M.P., Delogu, D., Ventura, R., 2012. Carta geologica d'Italia alla scala 1:100,000. WWW site. ISPRA. Via Vitaliano Brancati, 48 – 00144 Rome, Italy. URL: http://193.206.192.231/carta_geologica_italia/cartageologica.htm. in Italian.

Bornaetxea, T., Rossi, M., Marchesini, I., Alvioli, M., 2018. Effective surveyed area and its role in statistical landslide susceptibility assessments. *Natural Hazards and Earth System Sciences* 18, 2455–2469. doi:10.5194/nhess-18-2455-2018.

Bourrier, F., Dorren, L., Hungr, O., 2013. The use of ballistic trajectory and granular flow models in predicting rockfall propagation. *Earth Surface Processes and Landforms* 38, 435–440. doi:10.1002/esp.3372.

Bucci, F., Santangelo, M., Fongo, L., Marchesini, I., Alvioli, M., Cardinali, M., Melelli, L., 2021. Lithological map of Italy at 1:100,000 scale. Unpublished.

Buldyrev, S.V., Parshani, R., Paul, G., Stanley, H.E., Havlin, S., 2010. Catastrophic cascade of failures in interdependent networks. *Nature* 464, 1025–1028. doi:10.1038/nature08932.

Buyer, A., Aichinger, S., Schubert, W., 2020. Applying photogrammetry and semi-automated joint mapping for rock mass characterization. *Engineering Geology* 264, 105332. doi:10.1016/j.enggeo.2019.105332.

Camilo, D.C., Lombardo, L., Mai, P.M., Dou, J., Huser, R., 2017. Handling high predictor dimensionality in slope-unit-based landslide susceptibility models through lasso-penalized generalized linear model. *Environmental Modelling & Software* 97, 145–156. doi:10.1016/j.envsoft.2017.08.003.

Casagrande, L., Cavallini, P., Frigeri, A., Furieri, A., Marchesini, I., Neteler, M., 2007. GIS open source. Flaccovio, Palermo. In Italian.

Cats, O., Yap, M., van Oort, N., 2016. Exposing the role of exposure: Public transport network risk analysis. *Transportation Research Part A: Policy and Practice* 88, 1–14. doi:10.1016/j.tra.2016.03.015.

Chartrand, G., Chartrand, G., Lesniak, L., Lesniak, L., Zhang, P., 1993. *Graphs & Digraphs*. Chapman and Hall/CRC, Boca Raton, FL.

Chen, Z., Liang, S., Ke, Y., Yang, Z., Zhao, H., 2020. Landslide susceptibility assessment using different slope units based on the evidential belief function model. *Geocarto International* 35, 1641–1664. doi:10.1080/10106049.2019.1582716.

Cohen, R., Erez, K., ben Avraham, D., Havlin, S., 2000. Resilience of the internet to random breakdowns. *Physical Review Letters* 85, 4626–4628. doi:10.1103/PhysRevLett.85.4626.

Collins, B.D., Stock, G.M., 2016. Rockfall triggering by cyclic thermal stressing of exfoliation fractures. *Nature Geoscience* 9, 395–400. doi:10.1038/ngeo2686.

Corominas, J., Mavrouli, O., Ruiz-Carulla, R., 2018. Magnitude and frequency relations: are there geological constraints to the rockfall size? *Landslides* 15, 829–845. doi:10.1007/s10346-017-0910-z.

Delonca, A., Gunzburger, Y., Verdel, T., 2014. Statistical correlation between meteorological and rockfall databases. *Natural Hazards and Earth System Sciences* 14, 1953–1964. doi:10.5194/nhess-14-1953-2014.

Evans, S.G., Hungr, O., 1993. The assessment of rockfall hazard at the base of talus slopes. *Canadian Geotechnical Journal* 30, 620–636. doi:10.1139/t93-054.

Fongo, L., 2018. *Verso una nuova carta litologica d'Italia in scala 1:100,000*. (in Italian) Master Thesis, University of Perugia.

Freeman, L.C., 1978. Centrality in social networks conceptual clarification. *Social Networks* 1, 215–239. doi:10.1016/0378-8733(78)90021-7.

Giacomini, A., Thoeni, K., Santise, M., Diotri, F., Booth, S., Fityus, S., Roncella, R., 2020. Temporal-spatial frequency rockfall data from open-pit highwalls using a low-cost monitoring system. *Remote Sensing* 12, 2459. doi:10.3390/rs12152459.

Giordan, D., Adams, M.S., Aicardi, I., Alicandro, M., Allasia, P., Baldo, M., Berardinis, P.D., Dominici, D., Godone, D., Hobbs, P., Lechner, V., Niedzielski, T., Piras, M., Rotilio, M., Salvini, R., Segor, V., Sotier, B., Troilo, F., 2020. The use of unmanned aerial vehicles (uavs) for engineering geology applications. *Bulletin of Engineering Geology and the Environment* 79, 3437–3481. doi:10.1007/s10064-020-01766-2.

Govi, M., 1977. Photo-interpretation and mapping of the landslides triggered by the Friuli earthquake (1976). *Bulletin of the International Association of Engineering Geology* 15, 67–72. doi:10.1007/BF02592650.

Guzzetti, F., Crosta, G., Detti, R., Agliardi, F., 2002. STONE: a computer program for the three-dimensional simulation of rockfalls. *Computers & Geosciences* 28, 1079 – 1093. doi:10.1016/S0098-3004(02)00025-0.

Guzzetti, F., Gariano, S.L., Peruccacci, S., Brunetti, M.T., Marchesini, I., Rossi, M., Melillo, M., 2020. Geographical landslide early warning systems. *Earth-Science Reviews* 200, 102973. doi:10.1016/j.earscirev.2019.102973.

Guzzetti, F., Reichenbach, P., 1994. Towards a definition of topographic divisions for Italy. *Geomorphology* 11, 57–74. doi:10.1016/0169-555X(94)90042-6.

Guzzetti, F., Reichenbach, P., Ghigi, S., 2004. Rockfall hazard and risk assessment along a transportation corridor in the Nera Valley, Central Italy. *Environmental Management* 34, 191–208. doi:10.1007/s00267-003-0021-6.

Guzzetti, F., Reichenbach, P., Wieczorek, G.F., 2003. Rockfall hazard and risk assessment in the Yosemite Valley, California, USA. *Natural Hazards and Earth System Sciences* 3, 491–503. doi:10.5194/nhess-3-491-2003.

Hungr, O., Evans, S.G., Hazzard, J., 1999. Magnitude and frequency of rock falls and rock slides along the main transportation corridors of southwestern British Columbia. *Canadian Geotechnical Journal* 36, 224–238. doi:10.1139/t98-106.

ISPRA, 2018. Landslides and floods in Italy: hazard and risk indicators – Summary Report 2018. Technical report. The Institute for Environmental Protection and Research. Via Vitaliano Brancati, 48 – 00144 Rome, Italy. URL: <http://www.isprambiente.gov.it/287/bis/2018>.

Jaboyedoff, M., Oppikofer, T., Abellán, A., Derron, M.H., Loyer, A., Metzger, R., Pedrazzini, A., 2012. Use of LIDAR in landslide investigations: a review. *Natural Hazards* 61, 5–28. doi:10.1007/s11069-010-9634-2.

Jacobs, L., Kervyn, M., Reichenbach, P., Rossi, M., Marchesini, I., Alvioli, M., Dewitte, O., 2020. Regional susceptibility assessments with heterogeneous landslide information: Slope unit- vs. pixel-based approach. *Geomorphology* 356, 107084. doi:10.1016/j.geomorph.2020.107084.

Jiang, B., 2013. Head/tail breaks: A new classification scheme for data with a heavy-tailed distribution. *The Professional Geographer* 65, 482–494. doi:10.1080/00330124.2012.700499.

Katifori, E., Szöllösi, G.J., Magnasco, M.O., 2010. Damage and fluctuations induce loops in optimal transport networks. *Physical Review Letters* 104, 048704. doi:10.1103/PhysRevLett.104.048704.

Li, H., Li, X., Li, W., Zhang, S., Zhou, J., 2019. Quantitative assessment for the rockfall hazard in a post-earthquake high rock slope using terrestrial laser scanning. *Engineering Geology* 248, 1–13. doi:10.1016/j.enggeo.2018.11.003.

Li, L., Lan, H., 2020. Integration of spatial probability and size in slope-unit-based landslide susceptibility assessment: A case study. *International Journal of Environmental Research and Public Health* 17, 8055. doi:10.3390/ijerph17218055.

Lu, L., Zhang, M., 2013. Edge betweenness centrality, in: Dubitzky, W., Wolkenhauer, O., Cho, K.H., Yokota, H. (Eds.), *Encyclopedia of Systems Biology*. Springer New York, New York, NY, pp. 647–648. doi:10.1007/978-1-4419-9863-7_874.

Macciotta, R., Martin, C.D., Edwards, T., Cruden, D.M., Keegan, T., 2015. Quantifying weather conditions for rock fall hazard management. *Georisk: Assessment and Management of Risk for*

Engineered Systems and Geohazards 9, 171–186. doi:10.1080/17499518.2015.1061673.

Marchesini, I., Rossi, M., Alvioli, M., Santangelo, M., Cardinali, M., 2020. Slope–catchment area relationship for debris-flow source area identification, in: Alvioli, M., Marchesini, I., Melelli, L., Guth, P. (Eds.), Proceedings of the sixth Geomorphometry conference: Geomorphometry 2020, CNR Edizioni, Rome, Perugia, Italy. doi:10.30437/geomorphometry2020_47.

Marzorati, S., Luzi, L., De Amicis, M., 2002. Rock falls induced by earthquakes: a statistical approach. *Soil Dynamics and Earthquake Engineering* 22, 565–577. doi:10.1016/S0267-7261(02)00036-2.

Matas, G., Lantada, N., Corominas, J., Gili, J., Ruiz-Carulla, R., Prades, A., 2017. Simulation of full-scale rockfall tests with a fragmentation model. *Landslides* 14, 1565–1578. doi:10.1007/s10346-017-0818-7.

Matas, G., Lantada, N., Corominas, J., Gili, J., Ruiz-Carulla, R., Prades, A., 2020. Simulation of full-scale rockfall tests with a fragmentation model. *Geosciences* 10, 168. doi:10.3390/geosciences10050168.

Matasci, B., Stock, G.M., Jaboyedoff, M., Carrea, D., Collins, B.D., Guérin, A., Matasci, G., Ravanel, L., 2018. Assessing rockfall susceptibility in steep and overhanging slopes using three-dimensional analysis of failure mechanisms. *Landslides* 15, 859–878. doi:10.1007/s10346-017-0911-y.

Mattsson, L.G., Jenelius, E., 2015. Vulnerability and resilience of transport systems – a discussion of recent research. *Transportation Research Part A: Policy and Practice* 81, 16–34. doi:10.1016/j.tra.2015.06.002. resilience of Networks.

Mavrouli, O., Corominas, J., 2020. Evaluation of maximum rockfall dimensions based on probabilistic assessment of the penetration of the sliding planes into the slope. *Rock Mechanics and Rock Engineering* 53, 2301–2312. doi:10.1007/s00603-020-02060-z.

Melillo, M., Gariano, S., Peruccacci, S., Sarro, R., Mateos, R.M., Brunetti, M.T., 2020. Rainfall and rockfalls in the Canary Islands: assessing a seasonal link. *Natural Hazards and Earth System Sciences* 20, 2307–2317. doi:10.5194/nhess-20-2307-2020.

Melzner, S., Rossi, M., Guzzetti, F., 2020. Impact of mapping strategies on rockfall frequency-size distributions. *Engineering Geology* 272, 105639. doi:10.1016/j.engeo.2020.105639.

Menegoni, N., Giordan, D., Perotti, C., 2021. An open-source algorithm for 3d rock slope kinematic analysis (roka). *Applied Sciences* 11. doi:10.3390/app11041698.

Neteler, M., Mitasova, H., 2007. Open Source GIS: A GRASS GIS Approach. Springer, New York.

Peréz-Rey, I., Riquelme, A., González-deSantos, L.M., Estévez-Ventosa, X., Tomás, R., Alejano, L.R., 2019. A multi-approach rockfall hazard assessment on a weathered granite natural rock slope. *Landslides* 16, 2005–2015. doi:10.1007/s10346-019-01208-5.

Riquelme, A.J., Abellán, A., Tomás, R., Jaboyedoff, M., 2014. A new approach for semi-automatic rock mass joints recognition from 3D point clouds. *Computers & Geosciences* 68, 38–52. doi:10.1016/j.cageo.2014.03.014.

Rossi, M., Peruccacci, S., Brunetti, M.T., Marchesini, I., Luciani, S., Ardizzone, F., Balducci, V., Bianchi, C., Cardinali, M., Fiorucci, F., Mondini, A.C., Reichenbach, P., Salvati, P., Santangelo, M., Bartolini, D., Gariano, S.L., Palladino, M., Vessia, G., Viero, A., Andronico, L., Borselli, L., Deganutti, A.M., Iovine, G., Luino, F., Parise, M., Polemio, M., Guzzetti, F., Tonelli, G., 2012. SANF: National warning system for rainfall-induced landslides in Italy , in: Proceedings 11th Symposium on Landslides and 2nd North American Symposium on Landslides, Banff, Canada. pp. 1895–1899.

Rossi, M., Sarro, R., Reichenbach, P., Mateos, R.M., 2021. Probabilistic identification of rockfall source areas at regional scale in El Hierro (Canary Islands, Spain). *Geomorphology* 381, 107661. doi:10.1016/j.geomorph.2021.107661.

Ruiz-Carulla, R., Corominas, J., Gili, J.A., Matas, G., Lantada, N., Moya, J., Prades, A., Núñez Andrés, M.A., Buill, F., Puig, C., 2020. Analysis of fragmentation of rock blocks from real-scale tests. *Geosciences* 10, 308. doi:10.3390/geosciences10080308.

Santangelo, M., Alvioli, M., Baldo, M., Cardinali, M., Giordan, D., Guzzetti, F., Marchesini, I., Reichenbach, P., 2019. Brief communication: Remotely piloted aircraft systems for rapid emergency response: road exposure to rockfall in Villanova di Accumoli (Central Italy). *Natural Hazards and Earth System Sciences* 19, 325–335. doi:10.5194/nhess-19-325-2019.

Santangelo, M., Marchesini, I., Bucci, F., Cardinali, M., Cavalli, M., Crema, S., Marchi, L., Alvioli, M., Guzzetti, F., 2020. Exposure to landslides in rural areas in Central Italy. *Journal of Maps* 0, 1–9. doi:10.1080/17445647.2020.1746699.

Sarro, R., Mateos, R.M., Reichenbach, P., Aguilera, H., Riquelme, A., Hernández-Gutiérrez, L.E., Martín, A., Barra, A., Solar, L., Monserrat, O., Alvioli, M., Fernández-Merodo, J.A., López-Vinielles, J., Herrera, G., 2020. Geotechnics for rockfall assessment in the volcanic island of Gran Canaria (Canary Islands, Spain). *Journal of Maps* 16, 605–613. doi:10.1080/17445647.2020.1806125.

Schlögel, R., Marchesini, I., Alvioli, M., Reichenbach, P., Rossi, M., Malet, J.P., 2018. Optimizing landslide susceptibility zonation: Effects of DEM spatial resolution and slope unit delineation on logistic regression models. *Geomorphology* 301, 10–20. doi:10.1016/j.geomorph.2017.10.018.

Tacchia, D., 2004. Cartografia ufficiale geologica e geomorfologica. Technical report. ISPRA. Via Vitaliano Brancati, 48 – 00144 Rome, Italy. URL: <http://sg1.isprambiente.it/geologia100k/Documenti/cartuffgeo.pdf>. in Italian.

Tanyaş, H., Rossi, M., Alvioli, M., van Westen, C.J., Marchesini, I., 2019a. A global slope unit-based method for the near real-time prediction of earthquake-induced landslides. *Geomorphology* 327, 126–146. doi:10.1016/j.geomorph.2018.10.022.

Tanyaş, H., van Westen, C.J., Persello, C., Alvioli, M., 2019b. Rapid prediction of the magnitude scale of landslide events triggered by an earthquake. *Landslides* 16, 661–676. doi:10.1007/s10346-019-01136-4.

Tarquini, S., Isola, I., Favalli, M., Mazzarini, F., Bisson, M., Pareschi, M.T., Boschi, E., 2007. TINITALY/01: a new Triangular Irregular Network of Italy. *Annales Geophysicae* 50, 407–425. doi:10.4401/ag-4424.

Trigila, A., Iadanza, C., Spizzichino, D., 2010. Quality assessment of the Italian Landslide Inventory using GIS processing. *Landslides* 7, 455–470. doi:10.1007/s10346-010-0213-0.

Turanboy, A., Ülker, E., cüksütçü, C.B.K., 2018. A new approach for assessing stability of rock slopes considering centroids of weak zones. *Journal of Mining and Environment* 9, 1–18. doi:10.22044/jme.2017.5975.1414.

Velasquez, M., Hester, P.T., 2013. An analysis of multi-criteria decision making methods. *International Journal of Operations Research* 10, 56–66. URL: http://www.orstw.org.tw/ijor/vol10no2/ijor_vo10_no2_p67_p79.pdf.